

1 **MPeat – A fully coupled mechanical-ecohydrological model of peatland**  
2 **development**

3  
4 Adilan W. Mahdiyasa<sup>1,3\*</sup>, David J. Large<sup>1\*</sup>, Bagus P. Muljadi<sup>1</sup>, Matteo Icardi<sup>2</sup>, Savvas  
5 Triantafyllou<sup>4</sup>

6 <sup>1</sup>Department of Chemical and Environmental Engineering, University of Nottingham,  
7 University Park, Nottingham NG7 2RD, UK

8 <sup>2</sup>School of Mathematical Sciences, University of Nottingham, University Park, Nottingham  
9 NG7 2RD, UK

10 <sup>3</sup>Department of Mathematics, Bandung Institute of Technology, Bandung 40132, Indonesia

11 <sup>4</sup>Institute for Structural Analysis and Aseismic Research, School of Civil Engineering,  
12 National Technical University of Athens, Greece

13  
14 \* Corresponding author

15 adilan.mahdiyasa@nottingham.ac.uk; adilan@math.itb.ac.id (Adilan W. Mahdiyasa)

16 david.large@nottingham.ac.uk (David J. Large )

## ABSTRACT

17  
18  
19  
20  
21  
22  
23  
24  
25  
26  
27  
28  
29  
30  
31  
32  
33  
34  
35  
36  
37  
38  
39  
40

Mathematical models of long-term peatland development have been produced to analyse peatland behaviour. However, existing models ignore the mechanical processes that have the potential to provide important feedback. Here we propose a one-dimensional model, MPeat, that couples mechanical, ecological, and hydrological processes via poroelasticity theory, which couples fluid flow and solid deformation. Poroelasticity formulation in the MPeat is divided into two categories, fully saturated and unsaturated. To validate this formulation, we compare numerical solutions of the fully saturated case with analytical solutions of Terzaghi's problem. Two groups of MPeat simulations are run over 6000 years using constant and variable climate, and the results are compared to those of two other peat growth models, DigiBog and the Holocene Peat Model. Under both climatic conditions, MPeat generates the expected changes in bulk density, active porosity, and hydraulic conductivity at the transition from the unsaturated to the saturated zone. The range of values of peat physical properties simulated by MPeat show good agreement with field measurement, indicating plausible outputs of the proposed model. Compared to the other peat growth models, the results generated by MPeat illustrate the importance of poroelasticity to the behaviour of peatland. In particular, the inclusion of poroelasticity produces shallower water table depth, accumulates greater quantities of carbon, and buffers the effect of climate changes on water table depth and carbon accumulation rates. These results illustrate the importance of mechanical feedbacks on peatland ecohydrology and carbon stock resilience.

**Keywords:** peatland development; compression; ecohydrology; poroelasticity; effective stress; carbon stock

## INTRODUCTION

41

42 At a fundamental level, the compaction of water-saturated dead organic matter to form peat is  
43 a mechanical process. Yet, on account of numerical complexity and possibly strong  
44 ecohydrological focus, the previous models of peat growth do not incorporate mechanics. It is  
45 the purpose of this paper to present a fully coupled mechanical-ecohydrological model for peat  
46 growth and consider the potential implications of feedback within this model system.

47 Peatlands are complex systems (Belyea, 2009; Belyea & Baird, 2006) with the potential to shift  
48 dramatically between equilibrium states in response to environmental change, potentially  
49 releasing large quantities of carbon (Jackson et al., 2017; Loisel et al., 2017; Lunt et al., 2019;  
50 Yu et al., 2010). One approach to understanding this complex behaviour is through  
51 mathematical models that provide insight into the functioning of the peatland system on a wide  
52 range of timeframes and particularly beyond the timeframes of direct observation. These  
53 mathematical models of peatland development enable us to analyse nonlinear behaviour  
54 because of the internal feedback mechanisms (Hilbert et al., 2000; Morris et al., 2011) and the  
55 effects of past or future events on peatland carbon storage, for example, climate change  
56 (Heinemeyer et al., 2010; Ise et al., 2008; Yu et al., 2001) or drainage (Young et al., 2017).

57 The most advanced peatland development models are based on ecohydrological processes. For  
58 example, the one-dimensional Holocene Peat Model (HPM) (Frolking et al., 2010) groups  
59 peatland vegetation into 12 plant functional types (PFTs) based on their characteristics, the  
60 quantities of which are determined by the water table depth and nutrient status. Associated with  
61 each PFT is a productivity and a decomposition rate, the balance of which determines rates of  
62 peat accumulation. The effect of decomposition is tracked for each peat cohort in terms of the  
63 remaining mass, which in turn determines the bulk density, hydraulic conductivity, and  
64 porosity. DigiBog (Baird et al., 2012; Morris et al., 2012; Morris et al., 2011), a one, two or

65 three-dimensional peatland development model, is built on a series of coupled ecological and  
66 hydrological processes that are divided into plant litter production, decomposition, hydraulic  
67 properties, and a hydrological submodel. The hydrological submodel determines water table  
68 position and hence litter production and decomposition, which in turn affects hydraulic  
69 conductivity. However, bulk density and drainable porosity are held constant. The potential  
70 problem with this approach is that HPM, DigiBog, and similar models (e.g., Heinemeyer et al.,  
71 2010; Hilbert et al., 2000; Swinnen et al., 2019) ignore the mechanical cause of changes in peat  
72 physical properties that have the potential to influence the ecohydrology and peatland  
73 resilience. Examples of such mechanical effects that cannot be captured in these models include  
74 variable loading of the peat surface as productivity changes, the motion of the peat surface in  
75 response to changes in the height of the water table, and mechanical failure of the peat body.

76 Peat is a mechanically weak, poroelastic material due to its extremely high water content and  
77 void ratio with values ranging between 500% – 2000% and 7.5 – 30, respectively  
78 (Hanrahan, 1954; Hobbs, 1986, 1987; Mesri & Ajlouni, 2007). As a result, the changes in peat  
79 pore structure, which significantly influence hydraulic properties, are not only determined by  
80 progressive decomposition (Moore et al., 2005; Quinton et al., 2000) but also compression.  
81 Hydraulic conductivity decreases when the water table drops due to the mechanical  
82 deformation in the pore structure (Whittington & Price, 2006), an important process that can  
83 reduce water discharge from peatland. In a similar way, the enhancement of water input will  
84 expand the pore space that leads to an increase in hydraulic conductivity, promoting higher  
85 water loss from peatland. Swelling or shrinking of the pore space caused by mechanical  
86 deformation leads to the seasonal surface fluctuation, with the magnitude determined by several  
87 factors, such as Young's modulus, which is a measure of the stiffness of an elastic material,  
88 gas content, and loading effects (Glaser et al., 2004; Reeve et al., 2013).

89 In this paper, we present a new fully coupled one-dimensional mechanical, ecological, and  
90 hydrological peatland development model. Although the one-dimensional model is clearly a  
91 simplification of the real problem, it provides an insight into how our model simulates peatland  
92 as a complex system. The overall structure of the paper takes the form of three parts. The first  
93 part deals with the model formulation that provides detailed explanations about the governing  
94 equations and verification of the numerical method. This part also describes the changes in peat  
95 physical properties, including bulk density, active porosity (pores that actively transmit water  
96 (Hoag & Price, 1997)), hydraulic conductivity, and Young's modulus as part of the internal  
97 feedback mechanism. The second part presents model implementations and simulation results,  
98 which are run under two different cases, constant and non-constant climatic conditions. In the  
99 last part, we consider the implications of this model for peatland processes and discuss several  
100 aspects that can be developed to produce a more plausible model of peatland development.

101 Throughout the paper, we use the following precise definitions of the terms compaction,  
102 consolidation, and compression. Compaction is the reduction in volume due to the decrease in  
103 void space through the rearrangement of solid particles. If the volume reduction is caused by  
104 the expulsion of excess pore water pressure, it is called consolidation. The term compression  
105 refers to the process of applying inward or compressive forces to the material.

106

107

## **MODEL FORMULATION**

108 MPeat is conceptualised as a one-dimensional column of peat at the centre of a peatland with  
109 a new layer added every time step. As the peatland develops, its physical properties are affected  
110 by the feedback from the mechanical, ecological, and hydrological processes through the  
111 coupling between fluid flow and solid deformation, which is known as poroelasticity, and this  
112 is the essence of our model (Figure 1). Peatland accumulates carbon since peat production from

113 plant litter or organic matter is generally greater than peat decomposition. The rate of decay is  
114 high due to the unsaturated aerobic condition above the water table (unsaturated zone). In  
115 contrast, the condition is fully saturated below the water table (saturated zone), resulting in a  
116 low rate of anaerobic decay. Peat that is more decomposed becomes susceptible to deformation  
117 because of the decrease in strength and Young's modulus. This deformation affects the  
118 structure of pore space, represented by the change in bulk density, active porosity, and  
119 hydraulic conductivity. To accommodate this process, we define physical properties functions  
120 as follow

$$\rho = \rho(b, u, z) \quad (1)$$

$$\phi = \phi(b, u, z) \quad (2)$$

$$\kappa = \kappa(\phi) \quad (3)$$

$$E = E(\theta) \quad (4)$$

121 where  $\rho$  is the bulk density ( $\text{kg m}^{-3}$ ),  $\phi$  is the active porosity ( $-$ ),  $\kappa$  is the hydraulic  
122 conductivity ( $\text{m s}^{-1}$ ),  $E$  is the Young's modulus (Pa),  $b$  is the peatland height (m),  $u$  is the  
123 vertical displacement (m),  $z$  is the water table depth (m), and  $\theta$  is the remaining mass ( $-$ ).  
124 MPeat is divided into three submodels, mechanical, ecological, and hydrological as explained  
125 below.

126

### 127 **Mechanical submodel**

128 Peat can be viewed as a porous medium because it consists of solid particles from plant litter  
129 or organic matter, and the pores are filled with fluid. The total stresses that act on a porous  
130 medium are allocated to pore fluid and the solid skeleton. The first component leads to the  
131 excess pore fluid pressure, and the second component, termed the effective stress (Terzaghi,

132 1943), leads to the displacement of the solid. The effective stress is a part of the total stress  
133 defined as

$$\sigma' = \sigma - np \quad (5)$$

134 where  $\sigma'$  is the effective stress (Pa),  $\sigma$  is the total stress (Pa),  $n$  is the effective stress  
135 coefficient ( $-$ ), and  $p$  is the excess pore fluid pressure (Pa). The excess pore fluid pressure  
136 and the solid displacement can be solved simultaneously through the poroelasticity concept.

137 The poroelasticity formulation in the mechanical submodel is divided into two categories, i.e.,  
138 fully saturated and unsaturated, to accommodate the peatland characteristics. The fully  
139 saturated poroelasticity is developed to analyse the features of the saturated zone and follows  
140 Biot's theory of consolidation (Biot, 1941). For the one-dimensional case, the governing  
141 equations are explained as follows. The equation of equilibrium without body force has the  
142 following form

$$\frac{\partial \sigma}{\partial y} = 0 \quad (6)$$

143 where  $\sigma$  is the total stress (Pa). Equation (6) is obtained from Newton's law of motion, stating  
144 that in the absence of acceleration, all of the forces acting on a small element of material must  
145 balance.

146 The kinematic relation that links strain and displacement (Equation (7)), and the linear  
147 constitutive law that gives the relation between effective stress and strain (Equation (8)), can  
148 be written as

$$\epsilon = \frac{\partial u}{\partial y} \quad (7)$$

$$\sigma' = E\epsilon \quad (8)$$

149 where  $\epsilon$  is the strain ( $-$ ),  $u$  is the vertical displacement (m),  $\sigma'$  is the effective stress (Pa), and  
150  $E$  is the Young's modulus (Pa).

151 By introducing the conservation of mass of solid particles and water, together with Darcy's  
152 law for the flow of water in the porous medium, we can get

$$\alpha \frac{\partial \epsilon}{\partial t} + \frac{1}{M} \frac{\partial p_w}{\partial t} = \kappa \frac{\partial^2 p_w}{\partial y^2} \quad (9)$$

153 where  $\alpha$  is the Biot's coefficient ( $-$ ),  $\epsilon$  is the strain ( $-$ ),  $M$  is the Biot's modulus (Pa),  $p_w$  is  
154 the excess pore water pressure (Pa), and  $\kappa$  is the hydraulic conductivity ( $\text{m s}^{-1}$ ). The  
155 interpretation of Equation (9) is that the compression of a fully saturated porous medium  
156 consists of the compression of pore water, solid skeleton, and the amount of water expelled  
157 from it by the flow. The value of  $\alpha$  is equal to one (Terzaghi, 1943) and  $M$  is equal to the  
158 inverse of the specific storage, i.e.,  $M = \frac{1}{S_s}$  (Cheng, 2020; Green & Wang, 1990). In this  
159 formulation, the vertical head gradient is contained in the excess pore water pressure, which in  
160 turn influences the effective stress. Furthermore, the lower boundary is impermeable and  
161 experiences no displacement, while the upper boundary is fully drained.

162 In the unsaturated zone, water and air occupy the pore space. As the depth of the unsaturated  
163 zone is usually less than 0.5 m (Ballard et al., 2011; Ingram, 1982; Swinnen et al., 2019), we  
164 assume air pressure equal to atmospheric pressure. By making this assumption, Equation (9)  
165 can be extended to represent the unsaturated zone as

$$\alpha_w \frac{\partial \epsilon}{\partial t} + \frac{1}{M_w} \frac{\partial p_w}{\partial t} = \kappa \frac{\partial^2 p_w}{\partial y^2} \quad (10)$$

166 The parameters  $\alpha_w$  and  $M_w$  depend on the degree of saturation of water (Cheng, 2020)

$$\alpha_w = S_w \quad (11)$$



$$M_w = \frac{\gamma_w(1 - \lambda)}{\phi\lambda\mu} S_w^{-1/\lambda} (1 - S_w^{1/\lambda})^\lambda \quad (12)$$

167 where  $S_w$  is the degree of saturation of water (–),  $\gamma_w$  is the specific weight of water ( $\text{N m}^{-3}$ ),  
 168  $\phi$  is the active porosity (–),  $\lambda$  is the first water retention empirical constant (–),  $\mu$  is the  
 169 second water retention empirical constant ( $\text{m}^{-1}$ ),  $\epsilon$  is the strain (–),  $p_w$  is the excess pore  
 170 water pressure (Pa), and  $\kappa$  is the hydraulic conductivity ( $\text{m s}^{-1}$ ).

171 The mechanical submodel is described in terms of a partial differential equation with two  
 172 independent variables that are space  $y$  and time  $t$ , while ecological and hydrological submodels  
 173 only contain time  $t$  as an independent variable on their differential equation. To provide a fully  
 174 coupled model, the space discretisation in the mechanical submodel is obtained from the layer  
 175 thickness as follows

$$h = \frac{m}{\rho} \quad (13)$$

176 where  $h$  is the layer thickness (m),  $m$  is the peat mass per unit area ( $\text{kg m}^{-2}$ ) and  $\rho$  is the bulk  
 177 density ( $\text{kg m}^{-3}$ ).

178 Mechanical deformation of the peat body cannot be separated from water table depth, peat  
 179 production, and decomposition. Water table depth determines peat production and plant weight  
 180 at the top surface (see the Ecological submodel section below), which have a role as load  
 181 sources. Besides that, water table depth also influences the effective stress because a deeper  
 182 water table position leads to higher effective stresses and increases deformation. This process  
 183 reduces the void space and brings the solid particles into closer contact with one another  
 184 through vertical displacement, increasing the bulk density and decreasing active porosity

$$\rho_t = \rho_{t-1} \left( \frac{b_{t-1}}{b_{t-1} - u_{t-1}(1 + \beta z_{t-1})} \right) \quad (14)$$

$$\phi_t = \phi_{t-1} \left( \frac{b_{t-1} - u_{t-1}(1 + \beta z_{t-1})}{b_{t-1}} \right) \quad (15)$$

185 where  $\rho$  is the bulk density ( $\text{kg m}^{-3}$ ),  $\phi$  is the active porosity ( $-$ ),  $b$  is the peatland height  
 186 (m),  $u$  is the vertical displacement (m),  $\beta$  is the bulk density and active porosity parameter  
 187 ( $\text{m}^{-1}$ ), and  $z$  is the water table depth (m). The subscripts indicate the updated value of bulk  
 188 density and active porosity from the previous time. The other factor that affects mechanical  
 189 deformation significantly is decomposition. Zhu et al. (2020) showed that the decomposition  
 190 reduces the strength and Young's modulus of dead roots, one of the main constituents of peat  
 191 fibre. This result leads us to the conclusion that the Young's modulus should decrease as peat  
 192 decompose. For the initial model, we propose an equation that includes the effect of  
 193 decomposition on the peat Young's modulus as a linear function

$$E_t = \chi(1 + \theta_t^\zeta) \quad (16)$$

194 where  $E$  is the Young's modulus (Pa),  $\theta$  is the remaining mass ( $-$ ),  $\chi$  is the first Young's  
 195 modulus parameter (Pa) and  $\zeta$  is the second Young's modulus parameter ( $-$ ).

196

### 197 **Ecological submodel**

198 Peat production follows the equation from Morris et al. (2015), which depends not only on the  
 199 water table depth but also on the air temperature. This equation is the development of Belyea  
 200 & Clymo (2001) and can be written as

$$\psi = 0.001(9.3 + 133z - 0.022(100z)^2)^2(0.1575Temp + 0.0091),$$

$$\text{for } 0 \leq z \leq 0.668$$

$$\psi = 0,$$

(17)

for  $z > 0.668$

201 where  $\psi$  is the peat production ( $\text{kg m}^{-2} \text{ yr}^{-1}$ ),  $z$  is the water table depth (m),  $Temp$  is the air  
202 temperature ( $^{\circ}\text{C}$ ). Peat production has a strong relationship with above-ground biomass that  
203 can be used to model the plant weight at the top surface through the equation and data from  
204 Moore et al. (2002). To accommodate the wet condition of the plant that consists of shrub,  
205 sedge or herb, and *Sphagnum*, we multiply each type with a constant that is obtained from its  
206 water content. Thus, we may write the equation for plant weight

$$Y = c_1 \left( 10^{\frac{\log_{10}(\psi)+0.409}{0.985}} \right) (1 + d_1)g + c_2 (10^{\log_{10}(\psi)+0.001}) (1 + d_2)g \\ + (c_3 0.144) (1 + d_3)g \quad (18)$$

207 where  $Y$  is the plant weight (Pa),  $\psi$  is the peat production ( $\text{kg m}^{-2} \text{ yr}^{-1}$ ),  $g$  is the acceleration  
208 of gravity ( $\text{m s}^{-2}$ ),  $c_1, c_2, c_3$  are the plant proportions (–) and  $d_1, d_2, d_3$  are the constants for  
209 plant wet condition (–) with the indices 1, 2, 3 indicating shrub, sedge or herb, and *Sphagnum*,  
210 respectively. Besides peat production, the accumulation of mass in the peatland is also  
211 influenced by the decomposition process. It occurs in both zones, unsaturated and saturated,  
212 but at a different rate. If we assume that the rate of decay is constant at each zone, then the  
213 change of mass because of decay can be modelled as (Clymo, 1984)

$$\frac{dm}{dt} = -\eta m \quad (19)$$

214 where  $m$  is the mass per unit area ( $\text{kg m}^{-2}$ ) and  $\eta$  is the rate of decay ( $\text{yr}^{-1}$ ). Furthermore, the  
215 quotient between mass at time  $t$ , which has experienced decay, and the initial mass gives us  
216 the remaining mass of the peat, or formally

$$\theta_t = \frac{m_t}{m_0} \quad (20)$$

217 where  $\theta$  is the remaining mass (–),  $m_t$  is the mass per unit area at time  $t$  ( $\text{kg m}^{-2}$ ), and  $m_0$  is  
 218 the initial mass per unit area ( $\text{kg m}^{-2}$ ).

219

## 220 **Hydrological submodel**

221 The change in active porosity due to compression affects hydraulic conductivity because water  
 222 cannot move easily as the pore size becomes smaller. Therefore, one of the ways to model the  
 223 relationship between hydraulic conductivity and active porosity is

$$\kappa_t = \kappa_0 \left( \frac{\phi_t}{\phi_0} \right)^\xi \quad (21)$$

224 where  $\kappa$  is the hydraulic conductivity ( $\text{m s}^{-1}$ ),  $\kappa_0$  is the initial value of hydraulic conductivity  
 225 ( $\text{m s}^{-1}$ ),  $\phi$  is the active porosity (–),  $\phi_0$  is the initial value of active porosity (–), and  $\xi$  is the  
 226 hydraulic conductivity parameter (–). Because compression is influenced by decomposition  
 227 through Young's modulus (see Equation (16)), we can also interpret hydraulic conductivity in  
 228 Equation (21) as a function of decay. DigiBog also uses this interpretation to develop its  
 229 hydrophysical submodel (Baird et al., 2012; Morris et al., 2012).

230 The water table varies over time in response to the internal and external factors, including  
 231 change in the active porosity, hydraulic conductivity, peatland radius, and net rainfall. We  
 232 employ the equation from Childs (1969) (see also Swindles et al., 2012) to predict the water  
 233 table height at the centre of the peatland

$$\frac{d\Gamma}{dt} = \frac{r}{\phi} - \frac{2\kappa\Gamma^2}{l^2\phi} \quad (22)$$

234 where  $\Gamma$  is the water table height (m),  $r$  is the net rainfall ( $\text{m yr}^{-1}$ ),  $l$  is the peatland radius  
235 (m),  $\phi$  is the active porosity ( $-$ ), and  $\kappa$  is the hydraulic conductivity ( $\text{m s}^{-1}$ ). The difference  
236 between peatland height and water table height at time  $t$  result in the water table depth of the  
237 peatland, or mathematically

$$z = b - \Gamma \quad (23)$$

238 where  $z$  is the water table depth (m) and  $b$  is the peatland height (m). Water table height  
239 cannot exceed peatland height because we assume all the water will flow as surface water over  
240 the peatland area.

241

## 242 **Numerical formulation and verification**

243 Poroelasticity is used to couple mechanical, ecological, and hydrological submodels through  
244 the changes in peat physical properties, including bulk density, active porosity, hydraulic  
245 conductivity, and Young's modulus. These changes simultaneously affect the calculations from  
246 each submodel. Therefore, in the MPeat, each submodel does not run sequentially to obtain the  
247 final results.

248 MPeat ecological and hydrological submodels are solved using the finite difference method,  
249 which is similar to Morris et al. (2015) but with two main differences. First, the formulation  
250 and assumption to calculate the changes in peat physical properties. Second, the influence of  
251 air temperature on the decomposition process (see openly available MPeat simulation codes  
252 for detailed numerical formulation).

253 In this section, we focus on the numerical formulation and verification of MPeat mechanical  
254 submodel. We apply the finite element method (see Zienkiewicz et al., 2013) to approximate  
255 the solution of the mechanical submodel in which the primary variables are solid displacement

256 and excess pore water pressure. We compare the numerical solution of a fully saturated case  
 257 (Equation (6-9)) with the analytical solution of Terzaghi's problem to validate the finite  
 258 element algorithm. In this test case, a uniform vertical load  $q$  is applied on the top surface of a  
 259 fully saturated sample with height  $H$ . The boundary conditions are the same with mechanical  
 260 submodel formulation. If the initial value of excess pore water pressure is  $p_{w0}$  then

$$p_w(y, 0^+) = p_{w0} \quad (24)$$

$$\frac{dp_w}{dy} = 0, \text{ at } y = 0 \quad (25)$$

$$u(0, t) = 0 \quad (26)$$

$$p_w(H, t) = 0 \quad (27)$$

261 where  $p_w$  is the excess pore water pressure (Pa) and  $u$  is the vertical displacement (m). The  
 262 excess pore water pressure and vertical displacement are expressed as non-dimensional  
 263 quantities normalized excess pore water pressure  $P$  and degree of consolidation  $U$

$$P = \frac{p_w(y, t)}{p_{w0}} \quad (28)$$

$$U = \frac{u(y, t) - u(y, 0^+)}{u(y, \infty) - u(y, 0^+)} \quad (29)$$

264 The analytical solutions of Terzaghi's problem are (Biot, 1941; Verruijt, 2018; Wang, 2000)

$$P = \frac{4}{\pi} \sum_{k=1}^{\infty} \frac{(-1)^{k-1}}{2k-1} \cos \left[ (2k-1) \frac{\pi y}{2H} \right] \exp \left[ -(2k-1)^2 \frac{\pi^2 c_v t}{4 H^2} \right] \quad (30)$$

$$U = 1 - \frac{8}{\pi^2} \sum_{k=1}^{\infty} \frac{1}{(2k-1)^2} \exp \left[ -(2k-1)^2 \frac{\pi^2 c_v t}{4 H^2} \right] \quad (31)$$

$$c_v = \frac{\kappa}{S_s + \frac{\alpha^2}{K + (4/3)G}} \quad (32)$$

265 where  $P$  is the normalized excess pore water pressure (–),  $U$  is the degree of consolidation  
 266 (–),  $c_v$  is the consolidation coefficient ( $\text{m}^2 \text{s}^{-1}$ ),  $H$  is the sample height (m),  $\kappa$  is the  
 267 hydraulic conductivity ( $\text{m s}^{-1}$ ),  $S_s$  is the specific storage ( $\text{m}^{-1}$ ),  $\alpha$  is the Biot’s coefficient  
 268 (–),  $K$  is the bulk modulus (Pa), and  $G$  is the shear modulus (Pa).

269 We use 101 nodes and 100 elements to generate the simulation with the input data stated in  
 270 Table 1. The proposed algorithm shows good performance indicated by a small error between  
 271 numerical and analytical solutions (Figure 2). Furthermore, the mean absolute error for  
 272 normalized excess pore water pressure at the dimensionless time  $t^*$  equal to 0.01, 0.1, 0.5, and  
 273 1 are  $2.5 \times 10^{-3}$ ,  $6.3 \times 10^{-4}$ ,  $3.3 \times 10^{-5}$ , and  $2.7 \times 10^{-5}$ , respectively, with  $t^* = \frac{c_v t}{H^2}$ . The  
 274 mean absolute error for the degree of consolidation also shows a small value of  $3.9 \times 10^{-3}$ .

275

## 276 MODEL IMPLEMENTATION

277 To illustrate how MPeat works, we simulate peatland vertical growth with a fixed radius and  
 278 flat substrate for 6000 years using annual time steps. We assume that peat is an elastic material  
 279 (Waddington et al., 2010), with fluid flow through pore space following Darcy’s law. The  
 280 substrate properties are impermeable and stiff, so at the base layer the peat physical properties  
 281 are not affected by compression of the substrate. In this model, the load is associated with a  
 282 surficial peat addition (Equation (17)) and plant weight (Equation (18)), representing the  
 283 natural condition of the peatland.

284 We run two groups of simulations based on annual air temperature and net rainfall with the  
 285 parameter values summarised in Table 2. For the first group, we employ constant values for

286 those two variables that are  $6\text{ }^{\circ}\text{C}$  and  $0.8\text{ m yr}^{-1}$ , although this approach is not realistic, it gives  
287 baseline results and preliminary information to understand the model. Furthermore, this  
288 simplification is crucial for comparison purposes due to the high level of control of the model  
289 before proceeding to the next case. In the second group, we simulate the model using a more  
290 realistic climate, non-constant annual air temperature and net rainfall, developed from the  
291 sinusoidal function with some noise (Figure 3). We do not use the climate reconstruction model  
292 (e.g., Fischer & Jungclaus, 2011; Mauri et al., 2015; Pauling et al., 2006) because we want to  
293 keep it as simple as possible while also maintaining the effect of variable climate on the  
294 peatland growth over millennia.

295 We compare the simulation results of MPeat with DigiBog and HPM for peatland height,  
296 cumulative carbon, and water table depth under constant and non-constant climate. DigiBog  
297 parameters are obtained from Morris et al. (2015) except for the unsaturated zone decay rate,  
298 saturated zone decay rate, and initial bulk density, which are the same as MPeat values. HPM  
299 parameters, plant functional types, and formulation, which includes the effect of air  
300 temperature, are obtained from Frohking et al. (2010) and Treat et al. (2013), with the potential  
301 increase in bulk density  $\Delta\rho$  is equal to  $50\text{ kg m}^{-3}$ . For all three models, the cumulative carbon  
302 is formulated from cumulative organic mass multiplied by 40% of carbon content based on  
303 Loisel et al. (2014).

304 MPeat sensitivity analysis is conducted by changing the physical properties parameters of the  
305 model, i.e., Young's modulus parameters  $\chi$  and  $\zeta$ , and hydraulic conductivity parameter  $\xi$ . This  
306 is because field measurements of the Young's modulus and hydraulic conductivity of peat  
307 indicate that they have a wide range of values. We change the value of one parameter and all  
308 others remain the same as the baseline value (Table 2) for each simulation. Output variables  
309 examined from the sensitivity analysis include the value of bulk density, active porosity,  
310 hydraulic conductivity, Young's modulus, peatland height, and cumulative carbon.



311

312

## SIMULATION RESULTS

### 313 **Group 1: constant air temperature and net rainfall**

314 The changes of peat physical properties with respect to depth (Figure 4) show that they have  
315 similar patterns that are a rapid shift around the depth of the water table, evolving to a relatively  
316 constant value in the saturated zone. However, within the saturated zone the trend changes  
317 abruptly at depths below 3 m due to the formation of the unsaturated zone about 400 years  
318 after peatland initiation (Figure 5c, MPeat). In particular, below 3 m the bulk density value  
319 decreases dramatically while active porosity, hydraulic conductivity, and Young's modulus  
320 values experienced a significant increase.

321 Comparison of MPeat to DigiBog and HPM (Figure 5) illustrates that all models produce  
322 similar long-term trends but with a number of key differences. After 6000 years, peatland  
323 height estimated from MPeat (3.27 m) is lower than DigiBog (6.01 m) but relatively similar  
324 to HPM (3.25 m). MPeat simulates the highest cumulative carbon ( $123 \text{ kg C m}^{-2}$ ) compared  
325 to DigiBog ( $121 \text{ kg C m}^{-2}$ ) and HPM ( $120 \text{ kg C m}^{-2}$ ). MPeat also predicts the water table  
326 depth around 0.28 m in the final simulation year, while DigiBog and HPM predict around  
327 0.39 m and 0.29 m, respectively.

328

### 329 **Group 2: non-constant air temperature and net rainfall**

330 The fluctuations of air temperature and net rainfall provide a significant influence on the peat  
331 physical properties in the saturated zone. For example, the decrease in bulk density from 110  
332 to  $98 \text{ kg m}^{-3}$  at a depth about 2.79 to 2.42 m (Figure 6a), and over the same interval, an  
333 increase in active porosity (Figure 6b) and hydraulic conductivity (Figure 6c) from

334 approximately 0.36 to 0.41 and  $7.34 \times 10^{-8}$  to  $3.82 \times 10^{-7} \text{ m s}^{-1}$  respectively corresponds  
335 to an abrupt shift to a cooler and wetter climatic interval around 5000 – 4200 years BP (Figure  
336 3). The opposite patterns of bulk density, active porosity, and hydraulic conductivity occur at  
337 a depth about 2.42 to 2.13 m due to a warmer and drier climatic interval around 4200 – 3600  
338 years BP. The effect of climate change is less pronounced on Young's modulus due to its high  
339 fluctuations (Figure 6d). Young's modulus is controlled solely by the remaining mass, and  
340 peatland internal feedback mechanisms are likely to overwrite climate signal preservation  
341 contained in the remaining mass.

342 MPeat estimates lower peatland height than DigiBog (3.36 m vs. 5.99 m) but a greater  
343 peatland height than the HPM (3.36 m vs. 2.64 m) after 6000 years (Figure 7a). MPeat  
344 simulates the highest cumulative carbon ( $131 \text{ kg C m}^{-2}$ ), compared to DigiBog  
345 ( $120 \text{ kg C m}^{-2}$ ) and HPM ( $98 \text{ kg C m}^{-2}$ ) (Figure 7b), which is similar to those of Group 1.  
346 The range of water table depths simulated by MPeat, DigiBog, and HPM are 0.15 to  
347 0.38 m, 0.22 to 0.67 m, and 0.25 to 0.58 m, respectively, without including the initiation time  
348 when the unsaturated zone is not well developed (Figure 7c). Furthermore, water table depth  
349 simulated by DigiBog and HPM experiences sudden increases, particularly in the last 2000  
350 years, increases that are absent from the MPeat simulation.

351

## 352 **Sensitivity analysis**

353 Changing Young's modulus parameters ( $\chi$  and  $\zeta$ , Equation 16) revealed that the other physical  
354 properties as well as peatland height and cumulative carbon, are affected by the initial  
355 parameters that determine Young's modulus. Under constant climate (Figure 8), increasing the  
356 first Young's modulus parameter  $\chi$  to  $3 \times 10^5 \text{ Pa}$  resulted in a higher Young's modulus value  
357 to the range of  $5 \times 10^5 - 6 \times 10^5 \text{ Pa}$ , which in turn reduced the bulk density to 50 – 81

358  $\text{kg m}^{-3}$  but increased the active porosity and hydraulic conductivity to interval 0.49 – 0.8 and  
359  $6.65 \times 10^{-6} - 1 \times 10^{-2} \text{ m s}^{-1}$ , respectively. A stiffer peat is less affected by compression,  
360 which leads to lower water retention due to higher hydraulic conductivity. Therefore, by  
361 increasing  $\chi$  to  $3 \times 10^5 \text{ Pa}$ , peatland height and cumulative carbon decreased by about 16%  
362 and 33% compared to the baseline value after 6000 years (Figure 5, MPeat). On the other  
363 hand, increasing the second Young's modulus parameter  $\zeta$  to 0.15 resulted in the lower  
364 Young's modulus ( $3 \times 10^5 - 4 \times 10^5 \text{ Pa}$ ) and consequently higher bulk density (50 – 111  
365  $\text{kg m}^{-3}$ ) but lower active porosity (0.36 – 0.8) and hydraulic conductivity ( $6.32 \times 10^{-8} -$   
366  $1 \times 10^{-2} \text{ m s}^{-1}$ ). These conditions increased the peatland height and cumulative carbon by  
367 about 2% and 6% in the final simulation year.

368 Under non-constant climate (Figure 9), the influence of parameters  $\chi$  and  $\zeta$  on the output  
369 variables are similar to the constant climate case. Increasing  $\chi$  to  $3 \times 10^5 \text{ Pa}$  resulted in the  
370 lower bulk density (50 – 84  $\text{kg m}^{-3}$ ) but higher active porosity (0.47 – 0.8) and hydraulic  
371 conductivity ( $4.04 \times 10^{-6} - 1 \times 10^{-2} \text{ m s}^{-1}$ ). As a consequence, peatland height and  
372 cumulative carbon were reduced by about 17% and 34% compared to the baseline value after  
373 6000 years (Figure 7, MPeat). Changing  $\zeta$  to 0.15 increased bulk density (50 – 115  $\text{kg m}^{-3}$ )  
374 but decreased active porosity (0.35 – 0.8) and hydraulic conductivity ( $3.73 \times 10^{-8} -$   
375  $1 \times 10^{-2} \text{ m s}^{-1}$ ), which in turn resulted in higher peatland (3.42 m) and cumulative carbon  
376 ( $139 \text{ kg C m}^{-2}$ ) after 6000 years.

377 The hydraulic conductivity parameter ( $\xi$ , Equation 21) controls the decline of the hydraulic  
378 conductivity value as the active porosity becomes smaller due to the compression. Under  
379 constant climate, decreasing  $\xi$  to 12.5, which was associated with an increase in hydraulic  
380 conductivity value to the range of  $8.80 \times 10^{-7} - 1 \times 10^{-2} \text{ m s}^{-1}$ , reduced the peatland height  
381 by about 0.33 m and resulted in about  $13 \text{ kg C m}^{-2}$  lower cumulative carbon compared to the

382 baseline value after 6000 years. Under non-constant climate and  $\xi$  equal to 12.5, hydraulic  
383 conductivity increased to interval  $5.28 \times 10^{-7} - 1 \times 10^{-2} \text{ m s}^{-1}$ , which reduced peatland  
384 height and cumulative carbon by about 0.35 m and  $14 \text{ kg C m}^{-2}$  in the final simulation year.  
385 However, changing  $\xi$  had little impact on the other physical properties.

386

387

## DISCUSSION

388 Our results illustrate the influence of poroelastic deformation on the ecohydrological processes  
389 that lead to peat accumulation. As expected (Fenton, 1980; Quinton et al., 2000; Waddington  
390 et al., 2010; Whittington & Price, 2006), the most significant compaction in our model occurs  
391 at the transition from the unsaturated to the saturated zone. At this transition, peat experiences  
392 high effective stress due to unsaturated conditions. This results in the collapse of the pore  
393 structure, increasing bulk density and decreasing active porosity and hydraulic conductivity.  
394 The condition is different in the saturated zone where pore water pressure reduces the effective  
395 stress generating a relatively stable value of the physical properties (Figure 4a, 4b, and 4c).  
396 This finding is in line with expectations and field measurement from Price (2003), who  
397 observes that effective stress decreases substantially below the water table.

398 Because most of the mechanical deformation occurs in the unsaturated zone, MPeat illustrates  
399 how water table depth has a considerable impact on the peat physical properties. During  
400 warming and drying climatic events, as depth to the water table increases, the value of bulk  
401 density increases and active porosity and hydraulic conductivity decline (Figure 6a, 6b, and  
402 6c). As observed in the field (Price et al., 2003), this mechanical behaviour acts to reduce water  
403 loss and increase drought resilience. In addition, compression also reduces peat volume,  
404 causing the peatland surface to drop. This drop in the peat surface acts to maintain the relative  
405 position of the water table, which in turn helps sustain PFTs associated with wet surface

406 conditions (Schouten, 2002; Waddington et al., 2015). Conversely, a water surplus condition  
407 in the cooling and wetting period raises the water table, expands pore space, and decreases  
408 effective stress. This condition reduces bulk density and increases active porosity and hydraulic  
409 conductivity, leading to lower water retention and raising drainage potential. Such variations  
410 in peat physical properties within the saturated zone are routinely observed in cores and  
411 measured as dry bulk density. MPeat, therefore, has the capacity to model peat bulk density  
412 profiles in a way that can be compared to and complement other paleoclimatic indicators.

413

#### 414 **Comparison to other ecohydrological models**

415 MPeat, DigiBog, and HPM provide similar long-term trends of peatland development, which  
416 indicates they are capable of describing the general evolution of a peatland, including the  
417 changes in height, cumulative carbon, and water table depth. However, they have essential  
418 differences. The key difference between MPeat and DigiBog is the absence of poroelasticity  
419 (Table 3). In effect, DigiBog models a stiff peat in which the unsaturated zone cannot deform.  
420 This absence of dynamic expansion and compaction have the greatest consequence under a  
421 variable climate, with DigiBog sustaining a thicker unsaturated zone and consequently greater  
422 peat thickness and less cumulative carbon (Figure 7). To some extent, these discrepancies can  
423 be reduced by adjusting the parameter values, however as time progresses, the approach used  
424 in DigiBog will always tend to overestimate peatland height because it omits the effect of  
425 compression.

426 The difference between MPeat and HPM (Table 3) is somewhat less than with DigiBog, but  
427 this is primarily due to the empirical relationship used to predict the change in bulk density as  
428 a function of remaining mass (Frolking et al., 2010). However, the HPM is also an inherently  
429 stiffer model and as it evolves under a variable climate, tends to predict similar or deeper water

430 tables than MPeat and consequently less cumulative carbon. The empirical relationships used  
431 by HPM, therefore, limit our understanding of mechanical feedback mechanisms.

432 A final point of difference between the three models is that under variable climate, the outputs  
433 from MPeat are smoother than either DigiBog or HPM (Figure 7). This smoothness is a  
434 consequence of the mechanical buffering inherent to the poroelastic response to changes in  
435 excess precipitation and illustrates the potential importance of mechanics in maintaining the  
436 resilience of peatland systems. These results are in agreement with a study from Nijp et al.  
437 (2017), indicating that the inclusion of moss water storage and peat volume change because of  
438 mechanical deformation increase the projection of peatland drought resilience.

439 It can therefore be concluded that mechanical process plays a vital role in the peatland carbon  
440 stock (Figure 10). Compression provides negative feedback to an increasing water table depth  
441 (Waddington et al., 2015), which leads to the shorter residence time of plant litter in the  
442 unsaturated zone, increasing rates of carbon burial and reducing CO<sub>2</sub> emissions. The  
443 experiment from Blodau et al. (2004) corroborates this view and indicates that the production  
444 rate of CO<sub>2</sub> rises substantially with an increasing water table depth.

445

#### 446 **Comparison with field measurement**

447 A considerable uncertainty in the MPeat model is Young's modulus which in turn has the  
448 ability to influence the other physical properties as shown in the sensitivity analysis. Values of  
449 Young's modulus of peat are hard to measure in-situ and laboratory determined values are of  
450 questionable applicability in the field. For example, Dykes (2008) measured Young's modulus  
451 of Irish peat and obtained values ranging from  $1.15 \times 10^3$  to  $3.5 \times 10^3$  Pa and concluded that  
452 these very low values might be correlated with sample preparation that affected the strain  
453 measurement. As MPeat simulations evolve, Young's modulus values ranging between

454  $2.9 \times 10^5$  and  $6 \times 10^5$  Pa, far higher than the values provided by Dykes (2008). Nonetheless,  
455 according to Mesri & Ajlouni (2007), the ratio between Young's modulus with undrained shear  
456 strength lies in the range 20 – 80, and the reported data for undrained shear strength is in the  
457 range of  $4 \times 10^3$  –  $2 \times 10^4$  Pa, depending on the degree of humification and water content  
458 (Boylan et al., 2008; Long, 2005). Therefore, the plausible range of peat Young's modulus is  
459  $8 \times 10^4$  –  $1.6 \times 10^6$  Pa, the range value that is used in MPeat. As to the effect of decay on  
460 the Young's modulus of peat, this remains unknown beyond the expectation that decay should  
461 reduce elasticity within the range of reported values.

462 Some reassurance that the initial values of Young's modulus chosen in MPeat and subsequent  
463 values generated via decay are reasonable come from the comparison of the range of modelled  
464 and observed physical properties. Reported measurements of active porosity decrease with  
465 depth from as high as 0.8 near the top of the unsaturated zone to as low as 0.1 in the saturated  
466 zone (Hoag & Price, 1997; Quinton et al., 2000; Quinton et al., 2008; Siegel et al., 1995),  
467 similar to the MPeat active porosity pattern and values that range from 0.8 in the unsaturated  
468 zone to 0.34 in the saturated zone. Dry bulk density and hydraulic conductivity calculated in  
469 MPeat are between  $50$  –  $115 \text{ kg m}^{-3}$  and  $8.42 \times 10^{-9}$  –  $1 \times 10^{-2} \text{ m s}^{-1}$  broadly in line with  
470 reported measurements of dry bulk density and hydraulic conductivity around  $30$  –  $120$   
471  $\text{kg m}^{-3}$  and  $7 \times 10^{-9}$  –  $1.6 \times 10^{-2} \text{ m s}^{-1}$  (Clymo, 1984, 2004; Fraser et al., 2001; Hoag &  
472 Price, 1995; Hogan et al., 2006). Moreover, a considerable increase of hydraulic conductivity  
473 at the base of the peat profile obtained from MPeat, corresponding to peat accumulation under  
474 fully saturated conditions, is similar to some field observations (Clymo, 2004; Kneale, 1987;  
475 Waddington & Roulet, 1997). However, a notable difference between the modelled and  
476 measured peat physical properties is that the range of dry bulk densities generated by MPeat in  
477 the saturated zone is narrower than the range typically observed in many peat deposits. The  
478 most likely explanation for this is the constant initial value of Young's modulus, which in

479 reality will vary depending on PFT, with woody stemmed shrubs having a greater initial value  
480 than moss.

481

## 482 **Model limitations and future developments**

483 In one dimension, an alternative formulation that could address the limited range in dry bulk  
484 density would be to couple Young's modulus to PFT, shrub having a higher Young's Modulus  
485 and *Sphagnum* a lower Young's Modulus. This process requires a more generic peat  
486 production model that could be altered according to PFT, for example, the generalization of  
487 two-dimensional asymmetric Gaussian function from Frohking et al. (2010). In turn, the  
488 coupling between Young's modulus and PFT would generate a critical drying threshold below  
489 which shrub would become dominant, increasing stiffness in the peat and potentially acting as  
490 a positive feedback increasing carbon emissions and reducing the rate of carbon accumulation.  
491 Potentially this could be a natural threshold or tipping point in peatland evolution.

492 The effect of belowground structure, including shoots and roots of the vascular plants, could  
493 provide a supporting matrix that reduces the compression effect in the unsaturated zone  
494 (Malmer et al., 1994). This could be implemented in MPeat through Young's modulus equation  
495 which determines the ability of the peat to withstand compression. However, this process would  
496 increase model uncertainties because of the increasing number of free parameters. Therefore,  
497 a more complete sensitivity analysis that considers the interaction between parameters (e.g.,  
498 Quillet et al., 2013) would be helpful for the future development of the MPeat.

499 In one dimension, MPeat cannot capture the spatial variability of peat physical properties and  
500 thickness in a horizontal direction, yet many physical properties vary in two or three  
501 dimensions. For example, as shown by Lewis et al. (2012), the bulk density and hydraulic  
502 conductivity differ systematically between the centre of a peatland and its margin. Higher dry



503 bulk densities and lower hydraulic conductivities at the margins help peatland to hold the water  
504 and promote greater peat accumulation (Lapen et al., 2005). To understand these processes, it  
505 should be possible to extend MPeat into two or three dimensions. However, this extension is  
506 challenging because it increases the model complexities and becomes computationally  
507 expensive in terms of model run times. To achieve this, simplifying assumptions may be  
508 required, including turning off component parts of the model and exploring the mechanical  
509 behaviour of different bilayer peatland geometries. The approach should have considerable  
510 potential at improving our understanding of peat failure (mass movement), pipe formation and  
511 whether patterned pool systems have a mechanical origin. Indeed, the thresholds for  
512 mechanical failure of peat are also natural limits to carbon accumulation in a landscape and are  
513 tipping points for a notable natural hazard (Crisp et al., 1964; McCahon et al., 1987; Warburton  
514 et al., 2003).

515 Finally, another aspect that could be developed to produce a more plausible peatland growth  
516 model is the presence of gas bubbles. The entrapped gas bubbles block the pore space and  
517 affect the water flow, thus decreasing hydraulic conductivity (Baird & Waldron, 2003;  
518 Beckwith & Baird, 2001; Reynolds et al., 1992). Besides that, they have been shown to provide  
519 a noticeable effect on pore water pressure (Kellner et al., 2004), which in turn could influence  
520 effective stress. Introducing this aspect into the model requires a deep understanding of a  
521 complex peat pore structure, including the effect of dual-porosity, to determine the area where  
522 bubbles get trapped.

523

524

## CONCLUSION

525 MPeat is developed based on interactions among mechanical, ecological, and hydrological  
526 processes that are theoretically reasonable and empirically proven to occur in the real peatland.

527 These interactions influence peat physical properties, such as bulk density, active porosity,  
528 hydraulic conductivity, and Young's modulus through the coupling between fluid flow and  
529 solid deformation, which becomes the core of the model. MPeat illustrates the important  
530 function of poroelasticity in enhancing peatland resilience and sustaining peatland carbon stock  
531 in the face of climate change. The insights gained from this model may be of assistance to  
532 understand the long-term impact of climate change on the global carbon balance and the natural  
533 mechanical limits to peatland accumulation.

534

535

### **ACKNOWLEDGEMENTS**

536 We would like to thank Andy Baird and Nigel Roulet for interesting discussions on an earlier  
537 version of the model. This work was funded by the Directorate General of Higher Education  
538 (DIKTI) Indonesia, PhD scholarship awarded to AWM. We also thank Andy Reeve, Paul  
539 Morris, and anonymous reviewers for their insightful and constructive comments.

540

541

### **DATA AVAILABILITY**

542 The codes that support the findings of this study are openly available in zenodo at  
543 <https://doi.org/10.5281/zenodo.4786346> (Mahdiyasa, 2021).

544

545

### **CONFLICT OF INTEREST**

546 The authors declare no conflict of interest.

547

## REFERENCES

- 548
- 549 Baird, A. J., Morris, P. J., & Belyea, L. R. (2012). The DigiBog peatland development model 1:  
550 rationale, conceptual model, and hydrological basis. *Ecohydrology*, 5(3), 242-255.  
551 <https://doi.org/https://doi.org/10.1002/eco.230>
- 552
- 553 Baird, A. J., & Waldron, S. (2003). Shallow horizontal groundwater flow in peatlands is reduced by  
554 bacteriogenic gas production. *Geophysical Research Letters*, 30(20).  
555 <https://doi.org/https://doi.org/10.1029/2003GL018233>
- 556
- 557 Ballard, C. E., McIntyre, N., Wheater, H. S., Holden, J., & Wallage, Z. E. (2011). Hydrological modelling  
558 of drained blanket peatland. *Journal of Hydrology*, 407(1), 81-93.  
559 <https://doi.org/https://doi.org/10.1016/j.jhydrol.2011.07.005>
- 560
- 561 Beckwith, C. W., & Baird, A. J. (2001). Effect of biogenic gas bubbles on water flow through poorly  
562 decomposed blanket peat. *Water Resources Research*, 37(3), 551-558.  
563 <https://doi.org/https://doi.org/10.1029/2000WR900303>
- 564
- 565 Belyea, L. R. (2009). Nonlinear dynamics of peatlands and potential feedbacks on the climate system.  
566 In A. J. Baird, L. R. Belyea, X. Comas, A. Reeve, & L. D. Slater (Eds.), *Carbon Cycling in*  
567 *Northern Peatlands* (pp. 5-18). American Geophysical Union.  
568 <https://doi.org/https://doi.org/10.1029/2008GM000829>
- 569
- 570 Belyea, L. R., & Baird, A. J. (2006). Beyond the “limits to peat bog growth”: cross-scale feedback in  
571 peatland development. *Ecological Monographs*, 76(3), 299-322.  
572 [https://doi.org/https://doi.org/10.1890/0012-9615\(2006\)076\[0299:BTLPB\]2.0.CO;2](https://doi.org/https://doi.org/10.1890/0012-9615(2006)076[0299:BTLPB]2.0.CO;2)
- 573
- 574 Belyea, L. R., & Clymo, R. S. (2001). Feedback control of the rate of peat formation. *Proceedings of*  
575 *the Royal Society of London. Series B: Biological Sciences*, 268(1473), 1315-1321.  
576 <https://doi.org/doi:10.1098/rspb.2001.1665>
- 577
- 578 Biot, M. A. (1941). General theory of three-dimensional consolidation. *Journal of Applied Physics*,  
579 12(2), 155-164. <https://doi.org/10.1063/1.1712886>
- 580
- 581 Blodau, C., Basiliko, N., & Moore, T. R. (2004). Carbon turnover in peatland mesocosms exposed to  
582 different water table levels. *Biogeochemistry*, 67(3), 331-351.  
583 <https://doi.org/10.1023/B:BI0G.0000015788.30164.e2>
- 584
- 585 Boylan, N., Jennings, P., & Long, M. (2008). Peat slope failure in Ireland. *Quarterly Journal of*  
586 *Engineering Geology and Hydrogeology*, 41(1), 93-108. [https://doi.org/10.1144/1470-](https://doi.org/10.1144/1470-9236/06-028)  
587 [9236/06-028](https://doi.org/10.1144/1470-9236/06-028)
- 588
- 589 Cheng, A. H. D. (2020). A linear constitutive model for unsaturated poroelasticity by  
590 micromechanical analysis. *International Journal for Numerical and Analytical Methods in*  
591 *Geomechanics*, 44(4), 455-483. <https://doi.org/https://doi.org/10.1002/nag.3033>

592  
593 Childs, E. C. (1969). *An introduction to the physical basis of soil water phenomena*. John Wiley & Sons  
594 Ltd.

595  
596 Clymo, R. S. (1984). The limits to peat bog growth. *Philosophical Transactions of the Royal Society of*  
597 *London. B, Biological Sciences*, 303(1117), 605-654.  
598 <https://doi.org/doi:10.1098/rstb.1984.0002>

599  
600 Clymo, R. S. (2004). Hydraulic conductivity of peat at Ellergower Moss, Scotland. *Hydrological*  
601 *Processes*, 18(2), 261-274. <https://doi.org/https://doi.org/10.1002/hyp.1374>

602  
603 Crisp, D. T., Rawes, M., & Welch, D. (1964). A Pennine peat slide. *The Geographical Journal*, 130(4),  
604 519-524. <https://doi.org/10.2307/1792263>

605  
606 Dykes, A. P. (2008). Tensile strength of peat: laboratory measurement and role in Irish blanket bog  
607 failures. *Landslides*, 5(4), 417-429. <https://doi.org/10.1007/s10346-008-0136-1>

608  
609 Fenton, J. H. C. (1980). The rate of peat accumulation in Antarctic Moss Banks. *Journal of Ecology*,  
610 68(1), 211-228. <https://doi.org/10.2307/2259252>

611  
612 Fischer, N., & Jungclaus, J. H. (2011). Evolution of the seasonal temperature cycle in a transient  
613 Holocene simulation: orbital forcing and sea-ice. *Clim. Past*, 7(4), 1139-1148.  
614 <https://doi.org/10.5194/cp-7-1139-2011>

615  
616 Fraser, C. J. D., Roulet, N. T., & Moore, T. R. (2001). Hydrology and dissolved organic carbon  
617 biogeochemistry in an ombrotrophic bog. *Hydrological Processes*, 15(16), 3151-3166.  
618 <https://doi.org/https://doi.org/10.1002/hyp.322>

619  
620 Frohling, S., Roulet, N. T., Tuittila, E., Bubier, J. L., Quillet, A., Talbot, J., & Richard, P. J. H. (2010). A  
621 new model of Holocene peatland net primary production, decomposition, water balance,  
622 and peat accumulation. *Earth Syst. Dynam.*, 1(1), 1-21. [https://doi.org/10.5194/esd-1-1-](https://doi.org/10.5194/esd-1-1-2010)  
623 [2010](https://doi.org/10.5194/esd-1-1-2010)

624  
625 Glaser, P. H., Chanton, J. P., Morin, P., Rosenberry, D. O., Siegel, D. I., Ruud, O., Chasar, L. I., & Reeve,  
626 A. S. (2004). Surface deformations as indicators of deep ebullition fluxes in a large northern  
627 peatland. *Global Biogeochemical Cycles*, 18(1).  
628 <https://doi.org/https://doi.org/10.1029/2003GB002069>

629  
630 Green, D. H., & Wang, H. F. (1990). Specific storage as a poroelastic coefficient. *Water Resources*  
631 *Research*, 26(7), 1631-1637. <https://doi.org/https://doi.org/10.1029/WR026i007p01631>

632  
633 Hanrahan, E. T. (1954). An investigation of some physical properties of peat. *Géotechnique*, 4(3),  
634 108-123. <https://doi.org/10.1680/geot.1954.4.3.108>

635

636 Heinemeyer, A., Croft, S., Garnett, M. H., Gloor, E., Holden, J., Lomas, M. R., & Ineson, P. (2010). The  
637 MILLENNIA peat cohort model, predicting past, present and future soil carbon budgets and  
638 fluxes under changing climates in peatlands. *Climate Research*, 45(1), 207-226.  
639 <https://doi.org/10.3354/cr00928>

640  
641 Hilbert, D. W., Roulet, N., & Moore, T. (2000). Modelling and analysis of peatlands as dynamical  
642 systems. *Journal of Ecology*, 88(2), 230-242. [https://doi.org/https://doi.org/10.1046-j.1365-](https://doi.org/https://doi.org/10.1046/j.1365-2745.2000.00438.x)  
643 [2745.2000.00438.x](https://doi.org/https://doi.org/10.1046/j.1365-2745.2000.00438.x)

644  
645 Hoag, R. S., & Price, J. S. (1995). A field-scale, natural gradient solute transport experiment in peat at  
646 a Newfoundland blanket bog. *Journal of Hydrology*, 172(1), 171-184.  
647 [https://doi.org/https://doi.org/10.1016/0022-1694\(95\)02696-M](https://doi.org/https://doi.org/10.1016/0022-1694(95)02696-M)

648  
649 Hoag, R. S., & Price, J. S. (1997). The effects of matrix diffusion on solute transport and retardation in  
650 undisturbed peat in laboratory columns. *Journal of Contaminant Hydrology*, 28(3), 193-205.  
651 [https://doi.org/https://doi.org/10.1016/S0169-7722\(96\)00085-X](https://doi.org/https://doi.org/10.1016/S0169-7722(96)00085-X)

652  
653 Hobbs, N. B. (1986). Mire morphology and the properties and behaviour of some British and foreign  
654 peats. *Quarterly Journal of Engineering Geology and Hydrogeology*, 19(1), 7-80.  
655 <https://doi.org/10.1144/gsl.Qjeg.1986.019.01.02>

656  
657 Hobbs, N. B. (1987). A note on the classification of peat. *Géotechnique*, 37(3), 405-407.  
658 <https://doi.org/10.1680/geot.1987.37.3.405>

659  
660 Hogan, J. M., van der Kamp, G., Barbour, S. L., & Schmidt, R. (2006). Field methods for measuring  
661 hydraulic properties of peat deposits. *Hydrological Processes*, 20(17), 3635-3649.  
662 <https://doi.org/https://doi.org/10.1002/hyp.6379>

663  
664 Ingram, H. A. P. (1982). Size and shape in raised mire ecosystems: a geophysical model. *Nature*,  
665 297(5864), 300-303. <https://doi.org/10.1038/297300a0>

666  
667 Ise, T., Dunn, A. L., Wofsy, S. C., & Moorcroft, P. R. (2008). High sensitivity of peat decomposition  
668 to climate change through water-table feedback. *Nature Geoscience*, 1(11), 763-766.  
669 <https://doi.org/10.1038/ngeo331>

670  
671 Jackson, R. B., Lajtha, K., Crow, S. E., Hugelius, G., Kramer, M. G., & Piñeiro, G. (2017). The ecology of  
672 soil carbon: pools, vulnerabilities, and biotic and abiotic controls. *Annual Review of Ecology,*  
673 *Evolution, and Systematics*, 48(1), 419-445. [https://doi.org/10.1146/annurev-ecolsys-](https://doi.org/10.1146/annurev-ecolsys-112414-054234)  
674 [112414-054234](https://doi.org/10.1146/annurev-ecolsys-112414-054234)

675  
676 Kellner, E., Price, J. S., & Waddington, J. M. (2004). Pressure variations in peat as a result of gas  
677 bubble dynamics. *Hydrological Processes*, 18(13), 2599-2605.  
678 <https://doi.org/https://doi.org/10.1002/hyp.5650>

679

- 680 Kneale, P. E. (1987). Sensitivity of the groundwater mound model for predicting mire topography.  
681 *Hydrology Research*, 18(4-5), 193-202. <https://doi.org/10.2166/nh.1987.0014>
- 682
- 683 Lapen, D. R., Price, J. S., & Gilbert, R. (2005). Modelling two-dimensional steady-state groundwater  
684 flow and flow sensitivity to boundary conditions in blanket peat complexes. *Hydrological*  
685 *Processes*, 19(2), 371-386. <https://doi.org/https://doi.org/10.1002/hyp.1507>
- 686
- 687 Lewis, C., Albertson, J., Xu, X., & Kiely, G. (2012). Spatial variability of hydraulic conductivity and bulk  
688 density along a blanket peatland hillslope. *Hydrological Processes*, 26(10), 1527-1537.  
689 <https://doi.org/https://doi.org/10.1002/hyp.8252>
- 690
- 691 Loisel, J., van Bellen, S., Pelletier, L., Talbot, J., Hugelius, G., Karran, D., Yu, Z., Nichols, J., &  
692 Holmquist, J. (2017). Insights and issues with estimating northern peatland carbon stocks  
693 and fluxes since the Last Glacial Maximum. *Earth-Science Reviews*, 165, 59-80.  
694 <https://doi.org/https://doi.org/10.1016/j.earscirev.2016.12.001>
- 695
- 696 Loisel, J., Yu, Z., Beilman, D. W., Camill, P., Alm, J., Amesbury, M. J., Anderson, D., Andersson, S.,  
697 Bochicchio, C., Barber, K., Belyea, L. R., Bunbury, J., Chambers, F. M., Charman, D. J., De  
698 Vleeschouwer, F., Fiałkiewicz-Kozieł, B., Finkelstein, S. A., Gałka, M., Garneau, M.,  
699 Hammarlund, D., Hinchcliffe, W., Holmquist, J., Hughes, P., Jones, M. C., Klein, E. S., Kokfelt,  
700 U., Korhola, A., Kuhry, P., Lamarre, A., Lamentowicz, M., Large, D., Lavoie, M., MacDonald,  
701 G., Magnan, G., Mäkilä, M., Mallon, G., Mathijssen, P., Mauquoy, D., McCarroll, J., Moore, T.  
702 R., Nichols, J., O'Reilly, B., Oksanen, P., Packalen, M., Peteet, D., Richard, P. J., Robinson, S.,  
703 Ronkainen, T., Rundgren, M., Sannel, A. B. K., Tarnocai, C., Thom, T., Tuittila, E.-S., Turetsky,  
704 M., Väliranta, M., van der Linden, M., van Geel, B., van Bellen, S., Vitt, D., Zhao, Y., & Zhou,  
705 W. (2014). A database and synthesis of northern peatland soil properties and Holocene  
706 carbon and nitrogen accumulation. *The Holocene*, 24(9), 1028-1042.  
707 <https://doi.org/10.1177/0959683614538073>
- 708
- 709 Long, M. (2005). Review of peat strength, peat characterisation and constitutive modelling of peat  
710 with reference to landslides. *Studia Geotechnica et Mechanica*, 27(3-4), 67-90.
- 711
- 712 Lunt, P. H., Fyfe, R. M., & Tappin, A. D. (2019). Role of recent climate change on carbon  
713 sequestration in peatland systems. *Science of The Total Environment*, 667, 348-358.  
714 <https://doi.org/https://doi.org/10.1016/j.scitotenv.2019.02.239>
- 715
- 716 Mahdiyasa, A. W. (2021). *MPeat 1.0*. Zenodo.  
717 <https://doi.org/https://doi.org/10.5281/zenodo.4786346>
- 718
- 719 Malmer, N., Svensson, B. M., & Wallén, B. (1994). Interactions between Sphagnum mosses and field  
720 layer vascular plants in the development of peat-forming systems. *Folia Geobotanica &*  
721 *Phytotaxonomica*, 29(4), 483-496. <http://www.jstor.org/stable/4181306>
- 722
- 723 Mauri, A., Davis, B. A. S., Collins, P. M., & Kaplan, J. O. (2015). The climate of Europe during the  
724 Holocene: a gridded pollen-based reconstruction and its multi-proxy evaluation. *Quaternary*

725 *Science Reviews*, 112, 109-127.  
726 <https://doi.org/https://doi.org/10.1016/j.quascirev.2015.01.013>

727  
728 McCahon, C. P., Carling, P. A., & Pascoe, D. (1987). Chemical and ecological effects of a Pennine peat-  
729 slide. *Environmental Pollution*, 45(4), 275-289.  
730 [https://doi.org/https://doi.org/10.1016/0269-7491\(87\)90102-3](https://doi.org/https://doi.org/10.1016/0269-7491(87)90102-3)

731  
732 McNeil, P., & Waddington, J. M. (2003). Moisture controls on Sphagnum growth and CO2 exchange  
733 on a cutover bog. *Journal of Applied Ecology*, 40(2), 354-367.  
734 <https://doi.org/https://doi.org/10.1046/j.1365-2664.2003.00790.x>

735  
736 Mesri, G., & Ajlouni, M. (2007). Engineering properties of fibrous peats. *Journal of Geotechnical and*  
737 *Geoenvironmental Engineering*, 133(7), 850-866. [https://doi.org/doi:10.1061/\(ASCE\)1090-](https://doi.org/doi:10.1061/(ASCE)1090-0241(2007)133:7(850))  
738 [0241\(2007\)133:7\(850\)](https://doi.org/doi:10.1061/(ASCE)1090-0241(2007)133:7(850))

739  
740 Moore, T. R., Bubier, J. L., Frohling, S. E., Lafleur, P. M., & Roulet, N. T. (2002). Plant biomass and  
741 production and CO2 exchange in an ombrotrophic bog. *Journal of Ecology*, 90(1), 25-36.  
742 <https://doi.org/https://doi.org/10.1046/j.0022-0477.2001.00633.x>

743  
744 Moore, T. R., Trofymow, J. A., Siltanen, M., Prescott, C., & Group, C. W. (2005). Patterns of  
745 decomposition and carbon, nitrogen, and phosphorus dynamics of litter in upland forest and  
746 peatland sites in central Canada. *Canadian Journal of Forest Research*, 35(1), 133-142.  
747 <https://doi.org/10.1139/x04-149>

748  
749 Morris, P. J., Baird, A. J., & Belyea, L. R. (2012). The DigiBog peatland development model 2:  
750 ecohydrological simulations in 2D. *Ecohydrology*, 5(3), 256-268.  
751 <https://doi.org/https://doi.org/10.1002/eco.229>

752  
753 Morris, P. J., Baird, A. J., Young, D. M., & Swindles, G. T. (2015). Untangling climate signals from  
754 autogenic changes in long-term peatland development. *Geophysical Research Letters*,  
755 42(24), 10,788-710,797. <https://doi.org/https://doi.org/10.1002/2015GL066824>

756  
757 Morris, P. J., Belyea, L. R., & Baird, A. J. (2011). Ecohydrological feedbacks in peatland development:  
758 a theoretical modelling study. *Journal of Ecology*, 99(5), 1190-1201.  
759 <https://doi.org/https://doi.org/10.1111/j.1365-2745.2011.01842.x>

760  
761 Nijp, J. J., Metselaar, K., Limpens, J., Teutschbein, C., Peichl, M., Nilsson, M. B., Berendse, F., & van  
762 der Zee, S. E. A. T. M. (2017). Including hydrological self-regulating processes in peatland  
763 models: Effects on peatmoss drought projections. *Science of The Total Environment*, 580,  
764 1389-1400. <https://doi.org/https://doi.org/10.1016/j.scitotenv.2016.12.104>

765  
766 Pauling, A., Luterbacher, J., Casty, C., & Wanner, H. (2006). Five hundred years of gridded high-  
767 resolution precipitation reconstructions over Europe and the connection to large-scale  
768 circulation. *Climate Dynamics*, 26(4), 387-405. <https://doi.org/10.1007/s00382-005-0090-8>

769

770 Price, J. S. (2003). Role and character of seasonal peat soil deformation on the hydrology of  
771 undisturbed and cutover peatlands. *Water Resources Research*, 39(9).  
772 <https://doi.org/https://doi.org/10.1029/2002WR001302>

773  
774 Price, J. S., Heathwaite, A. L., & Baird, A. J. (2003). Hydrological processes in abandoned and restored  
775 peatlands: An overview of management approaches. *Wetlands Ecology and Management*,  
776 11(1), 65-83. <https://doi.org/10.1023/A:1022046409485>

777  
778 Quillet, A., Froking, S., Garneau, M., Talbot, J., & Peng, C. (2013). Assessing the role of parameter  
779 interactions in the sensitivity analysis of a model of peatland dynamics. *Ecological Modelling*,  
780 248, 30-40. <https://doi.org/https://doi.org/10.1016/j.ecolmodel.2012.08.023>

781  
782 Quinton, W. L., Gray, D. M., & Marsh, P. (2000). Subsurface drainage from hummock-covered  
783 hillslopes in the Arctic tundra. *Journal of Hydrology*, 237(1), 113-125.  
784 [https://doi.org/https://doi.org/10.1016/S0022-1694\(00\)00304-8](https://doi.org/https://doi.org/10.1016/S0022-1694(00)00304-8)

785  
786 Quinton, W. L., Hayashi, M., & Carey, S. K. (2008). Peat hydraulic conductivity in cold regions and its  
787 relation to pore size and geometry. *Hydrological Processes*, 22(15), 2829-2837.  
788 <https://doi.org/https://doi.org/10.1002/hyp.7027>

789  
790 Reeve, A. S., Glaser, P. H., & Rosenberry, D. O. (2013). Seasonal changes in peatland surface  
791 elevation recorded at GPS stations in the Red Lake Peatlands, northern Minnesota, USA.  
792 *Journal of Geophysical Research: Biogeosciences*, 118(4), 1616-1626.  
793 <https://doi.org/https://doi.org/10.1002/2013JG002404>

794  
795 Reynolds, W. D., Brown, D. A., Mathur, S. P., & Overend, R. P. (1992). Effect of in-situ gas  
796 accumulation on the hydraulic conductivity of peat. *Soil Science*, 153(5), 397-408.

797  
798 Schouten, M. G. C. (2002). *Conservation and restoration of raised bogs: Geological, hydrological, and*  
799 *ecological studies*. The Government Stationary Office.

800  
801 Siegel, D. I., Reeve, A. S., Glaser, P. H., & Romanowicz, E. A. (1995). Climate-driven flushing of pore  
802 water in peatlands. *Nature*, 374(6522), 531-533. <https://doi.org/10.1038/374531a0>

803  
804 Swindles, G. T., Morris, P. J., Baird, A. J., Blaauw, M., & Plunkett, G. (2012). Ecohydrological  
805 feedbacks confound peat-based climate reconstructions. *Geophysical Research Letters*,  
806 39(11). <https://doi.org/https://doi.org/10.1029/2012GL051500>

807  
808 Swinnen, W., Broothaerts, N., & Verstraeten, G. (2019). Modelling long-term blanket peatland  
809 development in eastern Scotland. *Biogeosciences*, 16(20), 3977-3996.  
810 <https://doi.org/10.5194/bg-16-3977-2019>

811  
812 Terzaghi, K. (1943). *Theoretical soil mechanics*. John Wiley & Sons, Inc.

813



- 814 Treat, C. C., Wisser, D., Marchenko, S., & Frolking, S. (2013). Modelling the effects of climate change  
815 and disturbance on permafrost stability in northern organic soil. *Mires and Peat*, 12.
- 816
- 817 Verruijt, A. (2018). Numerical and analytical solutions of poroelastic problems. *Geotechnical*  
818 *Research*, 5(1), 39-50. <https://doi.org/10.1680/jgere.15.00006>
- 819
- 820 Waddington, J. M., Kellner, E., Strack, M., & Price, J. S. (2010). Differential peat deformation,  
821 compressibility, and water storage between peatland microforms: Implications for  
822 ecosystem function and development. *Water Resources Research*, 46(7).  
823 <https://doi.org/https://doi.org/10.1029/2009WR008802>
- 824
- 825 Waddington, J. M., Morris, P. J., Kettridge, N., Granath, G., Thompson, D. K., & Moore, P. A. (2015).  
826 Hydrological feedbacks in northern peatlands. *Ecohydrology*, 8(1), 113-127.  
827 <https://doi.org/https://doi.org/10.1002/eco.1493>
- 828
- 829 Waddington, J. M., & Roulet, N. T. (1997). Groundwater flow and dissolved carbon movement in a  
830 boreal peatland. *Journal of Hydrology*, 191(1), 122-138.  
831 [https://doi.org/https://doi.org/10.1016/S0022-1694\(96\)03075-2](https://doi.org/https://doi.org/10.1016/S0022-1694(96)03075-2)
- 832
- 833 Wang, H. F. (2000). *Theory of linear poroelasticity with applications to geomechanics and*  
834 *hydrogeology*. Princeton University Press.
- 835
- 836 Warburton, J., Higgitt, D., & Mills, A. (2003). Anatomy of a Pennine peat slide, Northern England.  
837 *Earth Surface Processes and Landforms*, 28(5), 457-473.  
838 <https://doi.org/https://doi.org/10.1002/esp.452>
- 839
- 840 Whittington, P. N., & Price, J. S. (2006). The effects of water table draw-down (as a surrogate for  
841 climate change) on the hydrology of a fen peatland, Canada. *Hydrological Processes*, 20(17),  
842 3589-3600. <https://doi.org/https://doi.org/10.1002/hyp.6376>
- 843
- 844 Young, D. M., Baird, A. J., Morris, P. J., & Holden, J. (2017). Simulating the long-term impacts of  
845 drainage and restoration on the ecohydrology of peatlands. *Water Resources Research*,  
846 53(8), 6510-6522. <https://doi.org/https://doi.org/10.1002/2016WR019898>
- 847
- 848 Yu, Z., Campbell, I. D., Vitt, D. H., & Apps, M. J. (2001). Modelling long-term peatland dynamics. I.  
849 Concepts, review, and proposed design. *Ecological Modelling*, 145(2), 197-210.  
850 [https://doi.org/https://doi.org/10.1016/S0304-3800\(01\)00391-X](https://doi.org/https://doi.org/10.1016/S0304-3800(01)00391-X)
- 851
- 852 Yu, Z., Loisel, J., Brosseau, D. P., Beilman, D. W., & Hunt, S. J. (2010). Global peatland dynamics since  
853 the Last Glacial Maximum. *Geophysical Research Letters*, 37(13).  
854 <https://doi.org/https://doi.org/10.1029/2010GL043584>
- 855
- 856 Zhu, J., Wang, Y., Wang, Y., Mao, Z., & Langendoen, E. J. (2020). How does root biodegradation after  
857 plant felling change root reinforcement to soil? *Plant and Soil*, 446(1), 211-227.  
858 <https://doi.org/10.1007/s11104-019-04345-x>

859

860 Zienkiewicz, O. C., Taylor, R. L., & Zhu, J. Z. (2013). *The finite element method: its basis and*  
861 *fundamentals* (7th ed.). Elsevier.

862

863

864

865

866 **Table 1.** Input data for numerical and analytical solutions of Terzaghi's problem.

Name	Symbol	Value	Unit
Load	$q$	$1 \times 10^5$	Pa
Initial value of excess pore water pressure	$p_{w0}$	$1 \times 10^5$	Pa
Young's modulus	$E$	$1 \times 10^8$	Pa
Bulk modulus	$K$	$5.56 \times 10^7$	Pa
Shear modulus	$G$	$4.17 \times 10^7$	Pa
Hydraulic conductivity	$\kappa$	$1 \times 10^{-7}$	$\text{m s}^{-1}$
Specific storage	$S_s$	$1 \times 10^{-5}$	$\text{m}^{-1}$
Biot's coefficient	$\alpha$	1	-
Sample height	$H$	1	m

867

868

869 **Table 2.** Symbols and parameter default values for the simulations.

Name	Symbol	Value	Unit	Reference
Unsaturated zone decay rate	$\eta_{un}$	$5 \times 10^{-2}$	$\text{yr}^{-1}$	(Clymo, 1984)
Saturated zone decay rate	$\eta_{sa}$	$8 \times 10^{-5}$	$\text{yr}^{-1}$	(Clymo, 1984)
Biot's coefficient	$\alpha$	1	—	(Terzaghi, 1943)
Bulk density initial value	$\rho_0$	50	$\text{kg m}^{-3}$	(Lewis et al., 2012)
Carbon content	$C$	0.4	—	(Loisel et al., 2014)
Active porosity initial value	$\phi_0$	0.8	—	(Quinton et al., 2000)
Bulk density and active porosity parameter	$\beta$	1	$\text{m}^{-1}$	Present study
Hydraulic conductivity initial value	$\kappa_0$	$1 \times 10^{-2}$	$\text{m s}^{-1}$	(Hoag & Price, 1995)
Hydraulic conductivity parameter	$\xi$	15	—	Present study
Degree of saturation of water	$S_w$	0.4	—	Present study
Water retention empirical constant 1	$\lambda$	0.5	—	Present study
Water retention empirical constant 2	$\mu$	0.4	$\text{m}^{-1}$	Present study
Specific storage	$S_s$	$1.4 \times 10^{-2}$	$\text{m}^{-1}$	(Hogan et al., 2006)
Specific weight of water	$\gamma_w$	9800	$\text{N m}^{-3}$	(Cheng, 2020)
Peatland radius	$l$	500	m	Present study
Young's modulus parameter 1	$\chi$	$2 \times 10^5$	Pa	Present study
Young's modulus parameter 2	$\zeta$	0.1	—	Present study
Shrub proportion	$c_1$	0.61	—	(Moore et al., 2002)
Sedge or herb proportion	$c_2$	0.09	—	(Moore et al., 2002)
<i>Sphagnum</i> proportion	$c_3$	0.3	—	(Moore et al., 2002)

Shrub constant	$d_1$	0.4	–	Present study
Sedge or herb constant	$d_2$	0.4	–	Present study
<i>Sphagnum</i> constant	$d_3$	20	–	(McNeil & Waddington, 2003)
Gravitational acceleration	$g$	9.8	$\text{m s}^{-2}$	Present study

---

870

871

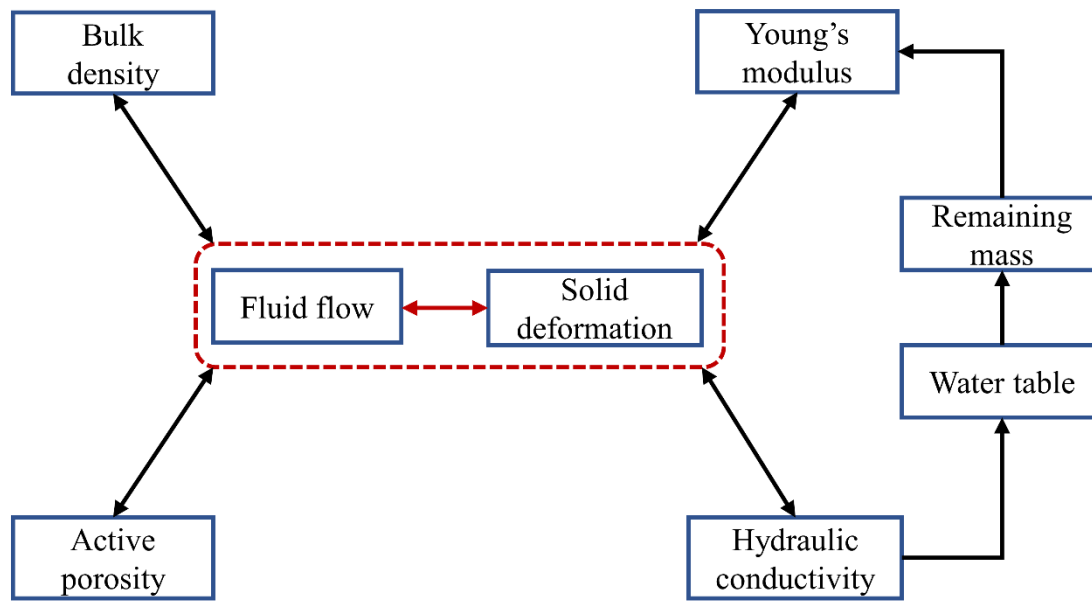
872

873 **Table 3.** The differences in approach for modelling peat physical properties among MPeat,  
 874 DigiBog, and HPM.

<b>MPeat</b>	<b>DigiBog</b>	<b>HPM</b>
Bulk density is a function of fluid flow and solid deformation.	Bulk density is a constant.	Bulk density is a function of remaining mass.
Active porosity is a function of fluid flow and solid deformation.	Drainable porosity is a constant.	Porosity is a function of peat bulk density and particle bulk density of organic matter.
Hydraulic conductivity is a function of active porosity.	Hydraulic conductivity is a function of remaining mass.	Hydraulic conductivity is a function of peat bulk density.
Young's modulus is a function of remaining mass.	-	-

875

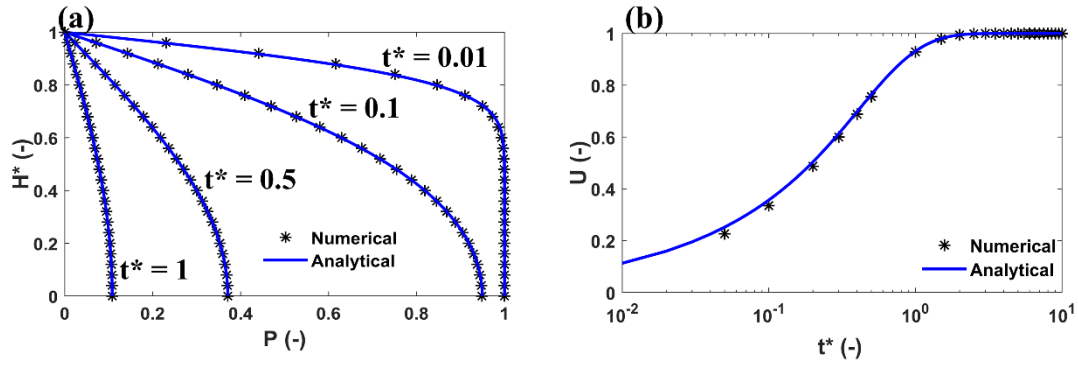
876



877

878 **Figure 1.** Schematic illustration of MPeat explains the interactions between peat physical  
 879 properties, including bulk density, active porosity, hydraulic conductivity, and Young's  
 880 modulus through the coupling between fluid flow and solid deformation.

881



882

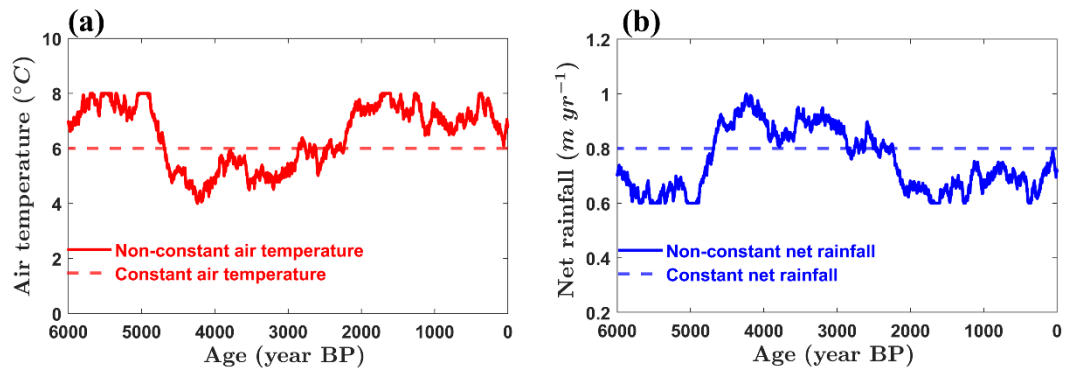
883 **Figure 2.** The comparison between numerical and analytical solutions of Terzaghi's problem.

884 Normalized pore water pressure  $P$  with normalized height  $H^* = \frac{y}{H}$  at various dimensionless

885 time  $t^*$  (a) and degree of consolidation  $U$  with dimensionless time  $t^*$  (b).

886





887

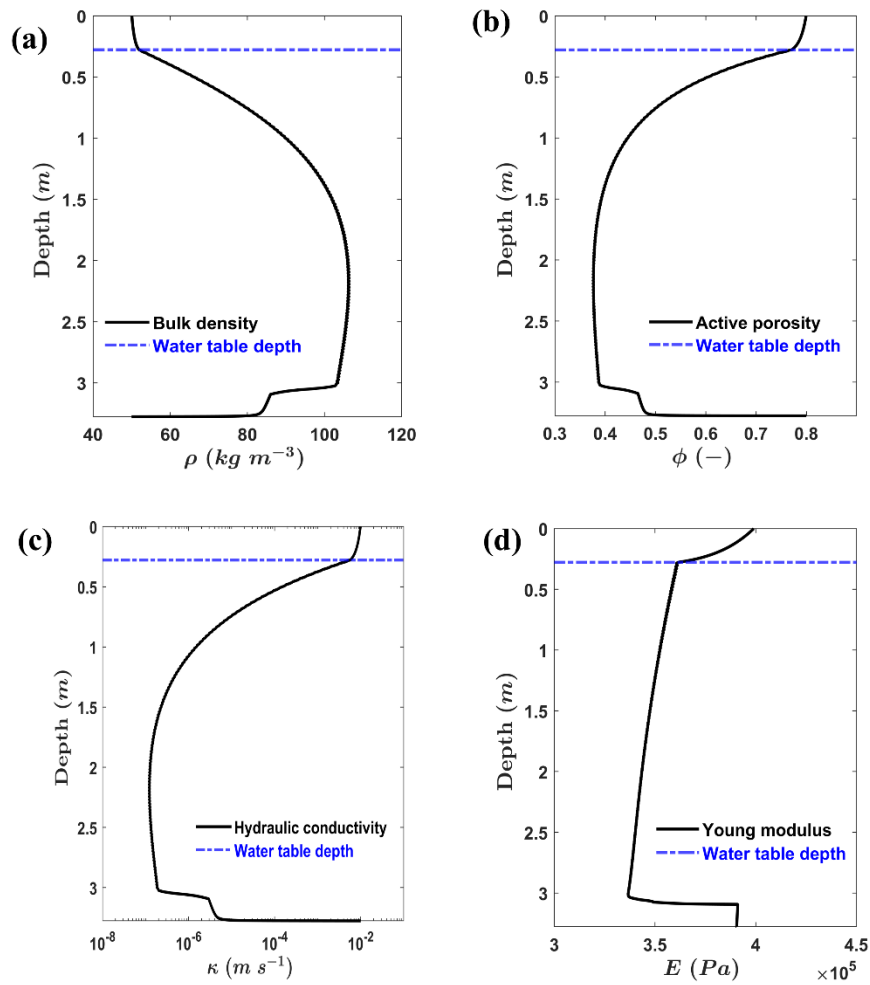
888 **Figure 3.** The constant and non-constant climate profile over 6000 years. In the constant case,

889 the value of air temperature (a) and net rainfall (b) are 6 °C and 0.8 m yr<sup>-1</sup>, while in the non-

890 constant case, the value of air temperature and net rainfall ranging between 4 °C – 8 °C and

891 0.6 m yr<sup>-1</sup> – 1 m yr<sup>-1</sup>.

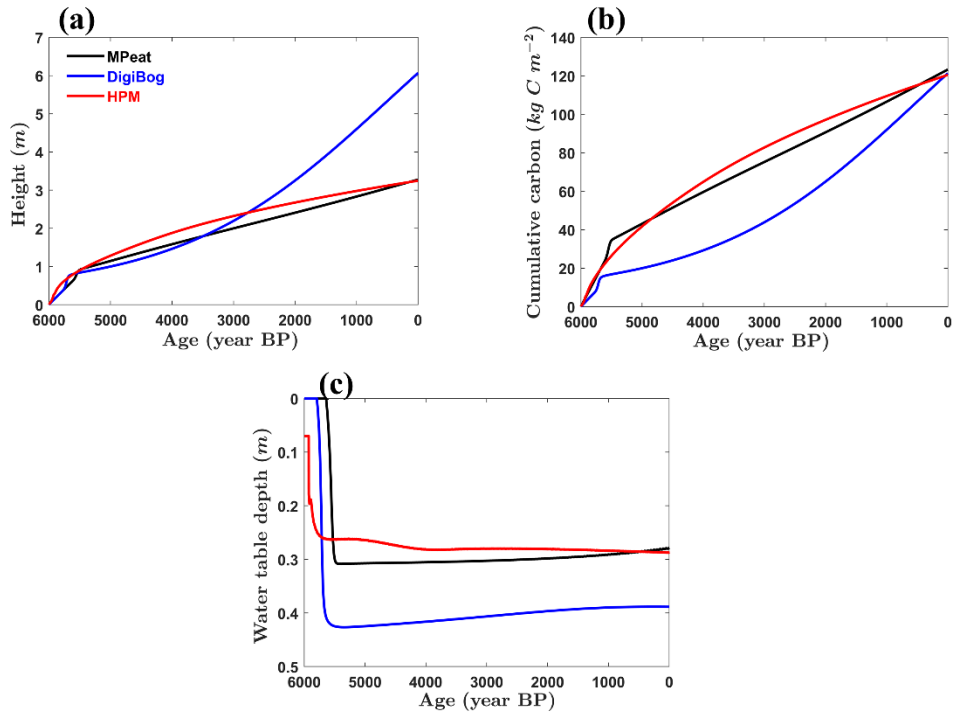
892



893

894 **Figure 4.** The profile of peat physical properties with depth, including bulk density (a), active  
 895 porosity (b), hydraulic conductivity (c), and Young's modulus (d) after 6000 simulated years  
 896 under constant climate.

897

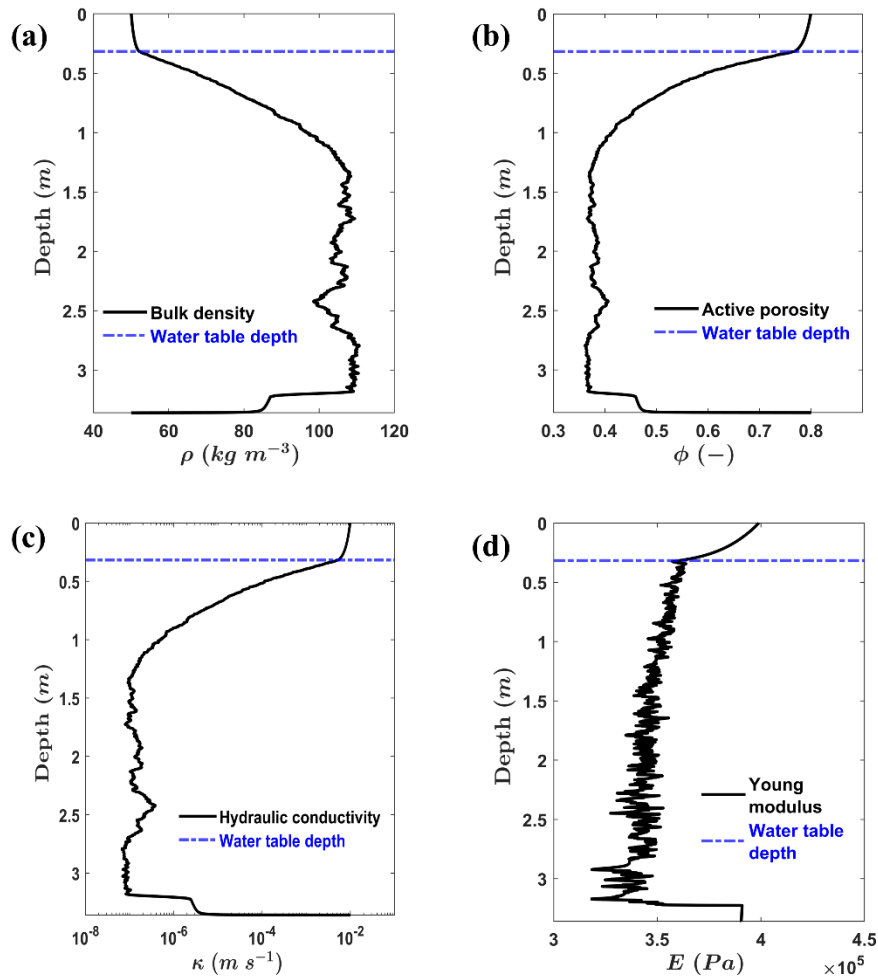


898

899 **Figure 5.** The comparison among MPeat, DigiBog, and HPM for peatland height (a),

900 cumulative carbon (b), and water table depth (c) under constant climate.

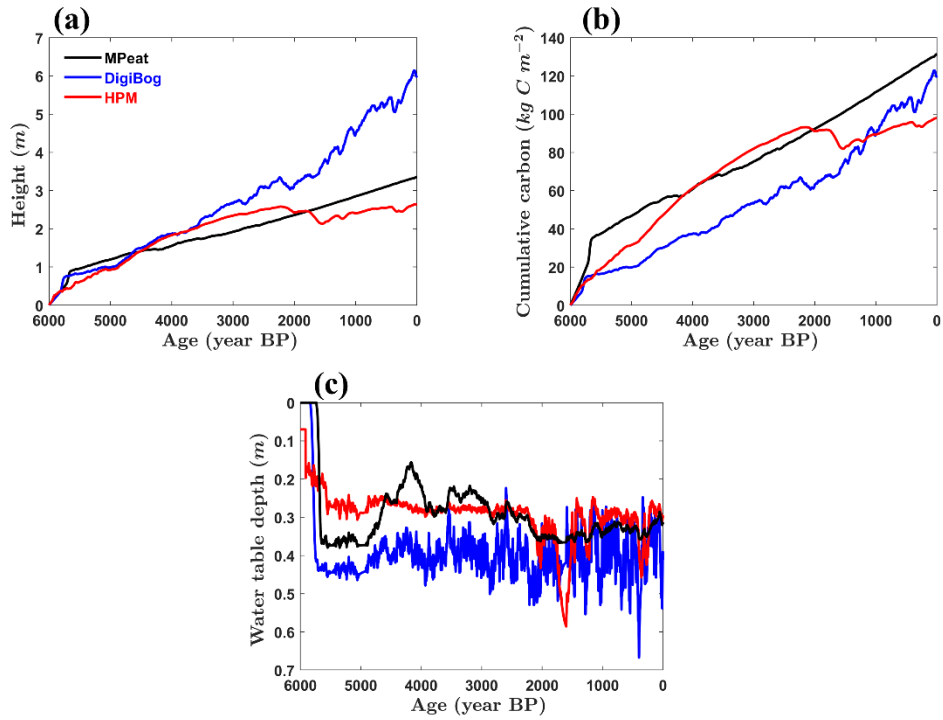
901



902

903 **Figure 6.** The profile of peat physical properties with depth, including bulk density (a), active  
 904 porosity (b), hydraulic conductivity (c), and Young's modulus (d) after 6000 simulated years  
 905 under non-constant climate.

906

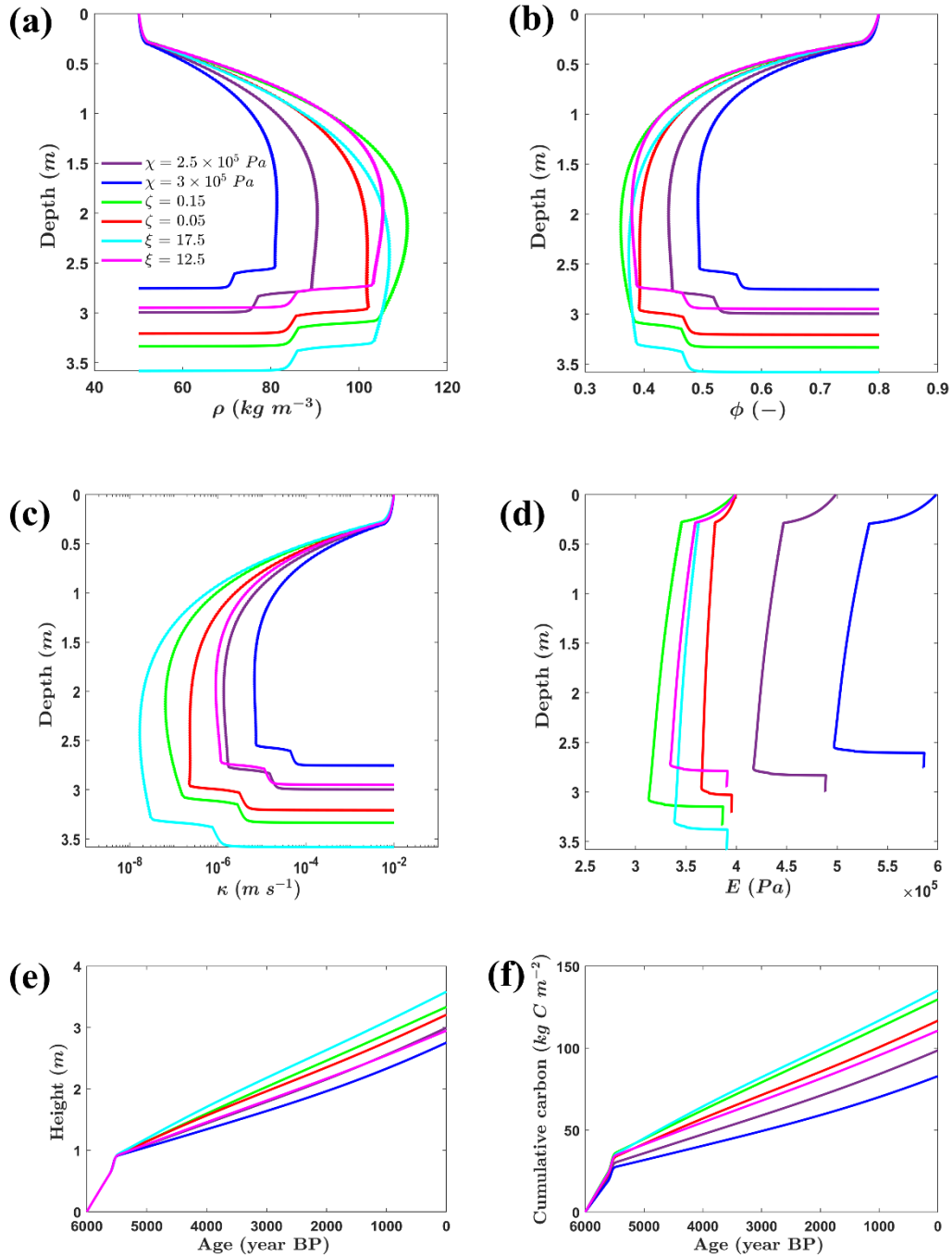


907

908 **Figure 7.** The comparison among MPeat, DigiBog, and HPM for peatland height (a),

909 cumulative carbon (b), and water table depth (c) under non-constant climate.

910



911

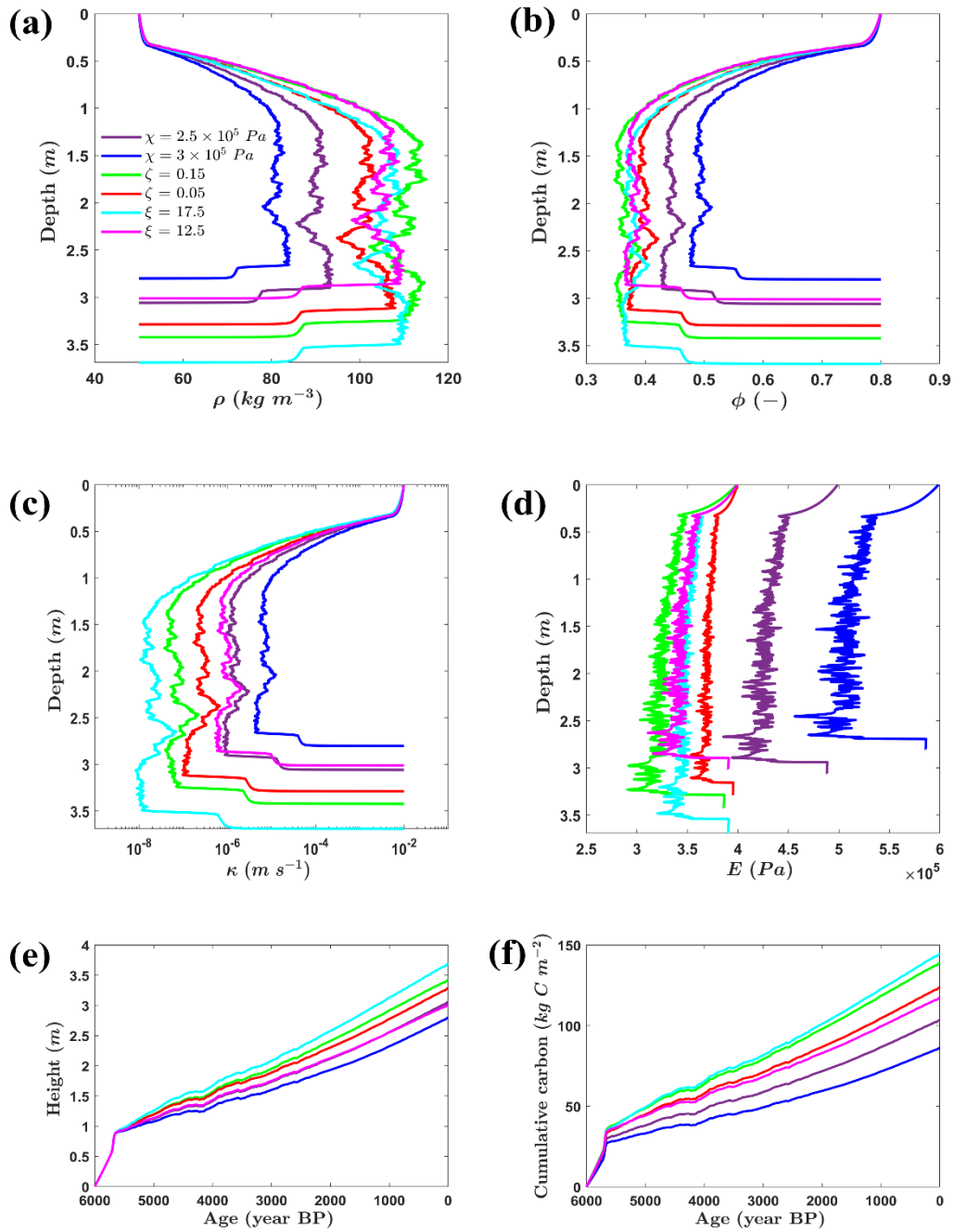
912 **Figure 8.** MPeat sensitivity analysis with the output variables including bulk density  $\rho$  (a),

913 active porosity  $\phi$  (b), hydraulic conductivity  $\kappa$  (c), Young's modulus  $E$  (d), peatland height

914 (e), and cumulative carbon (f) by changing the values of Young's modulus parameters  $\chi$  and

915  $\zeta$ , and hydraulic conductivity parameter  $\xi$  under constant climate. In the base runs (Figure 4

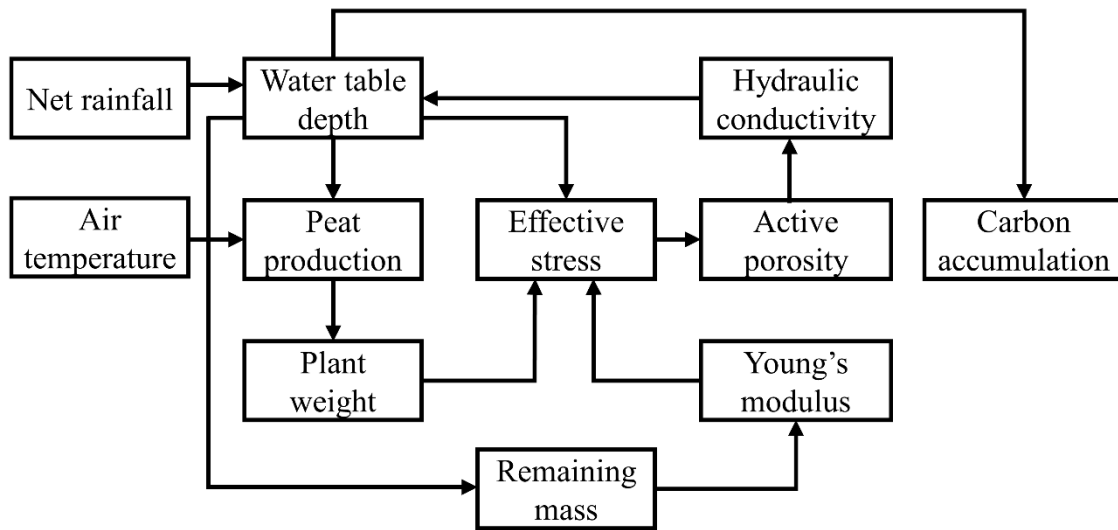
916 and 5, MPeat)  $\chi = 2 \times 10^5 \text{ Pa}$ ,  $\zeta = 0.1$ , and  $\xi = 15$ .



917

918 **Figure 9.** MPeat sensitivity analysis with the output variables including bulk density  $\rho$  (a),  
 919 active porosity  $\phi$  (b), hydraulic conductivity  $\kappa$  (c), Young's modulus  $E$  (d), peatland height  
 920 (e), and cumulative carbon (f) by changing the values of Young's modulus parameters  $\chi$  and  
 921  $\zeta$ , and hydraulic conductivity parameter  $\xi$  under non-constant climate. In the base runs (Figure  
 922 6 and 7, MPeat)  $\chi = 2 \times 10^5 \text{ Pa}$ ,  $\zeta = 0.1$ , and  $\xi = 15$ .

923



924

925 **Figure 10.** Overview of the influence of mechanics on peatland ecohydrology and carbon  
 926 stock resilience to the external perturbations, including the changes in net rainfall and air  
 927 temperature.